DISSERTATIONES
CHIMICAE
UNIVERSITATIS
TARTUENSIS
231

RITUMS CEPITIS

Modelling Structural and Geometrical Effects in Carbon Dioxide and Oxygen Electrocatalysis

DISSERTATIONES CHIMICAE UNIVERSITATIS TARTUENSIS
231

DISSERTATIONES CHIMICAE UNIVERSITATIS TARTUENSIS
231

RITUMS CEPITIS

Modelling Structural and Geometrical Effects in Carbon Dioxide and Oxygen Electrocatalysis

UNIVERSITY OF TARTU
Press
1632

Institute of Chemistry, Faculty of Science and Technology, University of Tartu, Estonia.

Dissertation has been accepted for the commencement of the degree of Doctor of Philosophy (PhD) in Chemistry on June 14, 2024 by the Council of the Institute of Chemistry, University of Tartu.

Supervisors

Assoc. Prof. Nadežda Kongi
University of Tartu
Estonia

Ph.D. Vladislav Ivaništšev
University of Tartu
Estonia

Opponent

Prof. Kai S. Exner
Faculty of Chemistry
University Duisburg-Essen
Germany

The public defense will take place on August 29, 2024 at 09:15 in Ravila 14a.

The publication of this dissertation was financed by the Institute of Chemistry, University of Tartu.

This work has been partially supported by ASTRA project PER ASPERA Graduate School of Functional Materials and Technologies receiving funding from the European Regional Development Fund under project in University of Tartu, Estonia.

ISSN 1406-0299 (print)
ISBN 978-9916-27-570-2 (print)
ISSN 2806-2159 (pdf)
ISBN 978-9916-27-571-9 (pdf)

University of Tartu Press
http://www.tyk.ee/

CONTENTS

1. List of abbreviations **7**

2. List of original publications **8**

3. Introduction **9**

4. Computational background **10**
4.1. Computational Hydrogen Electrode 10
4.2. Computational workflows 12
4.3. Atomic Simulation Environment builder 14
4.4. Density Functional Theory calculator 15
4.5. Technical aspects of calculations 16
4.6. Free energy diagram and predicted potentials 16

5. Structural effect in carbon dioxide electroreduction **19**
5.1. Literature overview 19
5.2. Structural models 20
5.3. Results and discussion 21
5.3.1. Summary and perspectives 24

6. Surface curvature effect in oxygen electrocatalysis **25**
6.1. Literature overview 25
6.1.1. Oxygen electrocatalysis 25
6.1.2. Scaling relations 25
6.2. Surface curvature effect 27
6.2.1. Flat or curved? 27
6.2.2. Effect of curvature 28
6.2.3. Modelling surface curvature effect 29
6.2.4. Results of surface curvature effect 31
6.2.5. Summary and perspectives 34
6.3. Geometry adaptive catalysts 35
6.3.1. Static or geometry adaptive? 35
6.3.2. Results of geometry adaptive catalysis 35
6.3.3. Pareto analysis 37
6.3.4. Summary and perspectives 38

7. Conclusion **39**

Bibliography **40**

Acknowledgements **47**

Sisukokkuvõte (Summary in Estonian) **48**

Publications **49**

CO_2 reduction to formate on an affordable bismuth metal-organic framework based catalyst. 51

Surface curvature effect on dual-atom site oxygen electrocatalysis. . . . 65

Bypassing the scaling relations in oxygen electrocatalysis with geometry-adaptive catalysts. 73

Curriculum Vitae **84**

Elulookirjeldus (Curriculum Vitae in Estonian) **86**

1. LIST OF ABBREVIATIONS

Acronyms

BEE Bayesian error estimation.
CcO cytochrome *c* oxidase.
CCS carbon capture and storage.
CCU carbon capture and utilisation.
CHE computational hydrogen electrode.
CNTs carbon nanotubes.
CO_2RR CO_2 reduction reaction.
DASs dual atom sites.
DF density functionals.
DFT density functional theory.
ESC energy storage and conversion.
FED free energy diagram.
HER hydrogen evolution reaction.
HOR hydrogen oxidation reaction.
M–N–C metal–nitrogen–carbon.
ML machine learning.
MM molecular mechanics.
MOF metal-organic framework.
NEB nudged elastic band.
NPs nanoparticles.
OER oxygen evolution reaction.
ORR oxygen reduction reaction.
PGMs platinum group metals.
RHE reversible hydrogen electrode.
SASs single atom sites.

Nomenclature

$U_{\mathbf{lim}}$ – the limiting potential, the lowest potential required to make all electrochemical steps downhill in energy.

η – overpotential, a deviation from the equilibrium potential.

ASE – software for setting up, manipulating, running, visualising, and analysing atomistic data in Atomic Simulation Environment (ASE).

GPAW – software for electronic structure calculations using Grid-based Projector-Augmented Waves (GPAW).

2. LIST OF ORIGINAL PUBLICATIONS

I Avila-Bolivar, B.*, **Cepitis, R.***, Alam, M., Assafrei, J.-M., Ping, K., Aruväli, J., Kikas, A., Kisand, V., Vlassov, S., Käärik, M., Leis, J., Ivaništšev, V., Starkov, P., Montiel, V., Solla-Gullon, J. & Kongi, N. CO_2 Reduction to Formate on an Affordable Bismuth Metal-Organic Framework Based Catalyst. *Journal of CO2 Utilization* **59**, 101937 (2022).
* – Contributed equally to this work.

II **Cepitis, R.**, Kongi, N., Rossmeisl, J. & Ivaništšev, V. Surface Curvature Effect on Dual-Atom Site Oxygen Electrocatalysis. *ACS Energy Letters* **8**, 1330–1335 (2023).

III **Cepitis, R.**, Ivaništšev, V., Rossmeisl, J. & Kongi, N. Bypassing the Scaling Relations in Oxygen Electrocatalysis with Geometry-Adaptive Catalysts. *Catalysis Science & Technology* **14**, 2105-2113 (2024).

Author's contributions:

Paper I DFT methodology. DFT calculations. DFT part manuscript writing.
Paper II Methodology. Calculations. Analysis. Manuscript draft.
Paper III Methodology. Calculations. Analysis. Manuscript draft.

3. INTRODUCTION

The *structure* and *geometry* are similar yet different concepts. In the following discussion, by *structure*, we understand an immutable set of connections of atoms that are chemically unchanging through the reaction. Therefore, the *structure* is a discrete quantity that constrains the activity and selectivity of electrocatalysis. In contrast, *geometry* is the spatial arrangement of the atoms within the fixed *structure* and can be surprisingly flexible. The intrinsic nature of the *geometry* to adapt provides an excellent opportunity to affect electrocatalytic behaviour in a continuous fashion.

From a modelling perspective, we can understand both *structure* and *geometry* through their *effects* on reactions.

- First, I describe the *structural effect* on electrocatalysis of CO_2 reduction reaction. The performed calculations allow us to predict the selectivity of active sites (also observable via structural characterisation), thus *explaining* observed experimental results.
- Second, I explore the *geometrical effect* on electrocatalysis of the oxygen reduction reaction. The modelled *geometrical effect* reveals a control over the activity and a possibility for bypassing the scaling relations, which, upon experimental confirmation, can break through the current limits in oxygen electrocatalysis.

4. COMPUTATIONAL BACKGROUND

The standard in computational methodology in modern electrocatalysis was established in the 2000s in a series of publications by the Danish school of electrocatalysis [1–6]. Descendant methods utilise the computational hydrogen electrode (CHE) as the reference in predicting catalytic activity and selectivity. With the exponential increase in computing power, CHE approaches have become affordable to many researchers, who can now calculate models from classical papers within minutes on their laptops. The low computational cost and acceptable predictive ability are the main reasons why CHE continues to lead the competition with alternative approaches, such as generalised computational hydrogen electrode and grand canonical ensemble modelling [7–10]. Recent reviews list the successes and challenges of CHE-based approaches [11–13], yet they avoid explaining technical details like in best practice protocols for modelling [14, 15].

This chapter introduces our CHE-based computational approach (as used in Papers I–III) with details on models, theory, and technical aspects.

4.1. Computational Hydrogen Electrode

The CHE-based approaches are applicable when a reaction can be written in terms of proton–electron ($H^+ + e^-$) transfer: $A + z(H^+ + e^-) \rightleftharpoons H_zA$. For example, in the following reversible reactions involving H_2, O_2, and CO_2:

$$2\,(H^+ + e^-) \rightleftharpoons H_2 \tag{4.1}$$

$$O_2 + 4\,(H^+ + e^-) \rightleftharpoons 2\,H_2O \tag{4.2}$$

$$CO_2 + 2\,(H^+ + e^-) \rightleftharpoons CO + H_2O \tag{4.3}$$

$$CO_2 + 2\,(H^+ + e^-) \rightleftharpoons HCOOH \tag{4.4}$$

These equations describe equilibrium in the hydrogen evolution reaction (HER) and the hydrogen oxidation reaction (HOR) [3, 16], the oxygen reduction reaction (ORR) and the oxygen evolution reaction (OER) [17, 18], and the CO_2 reduction reaction (CO_2RR) [19].

The CHE refers to the chemical potential of the proton in solution (μ_{H^+}) and electron at the Fermi level of the electrode (μ_{e^-}). At equilibrium conditions:

$$\frac{1}{2}\mu_{H_2} = \mu_{H^+} + \mu_{e^-} + eU_{RHE} \tag{4.5}$$

where μ_{H_2} is the chemical potential of H_2 gas at standard temperature and pressure, and U_{RHE} is the potential difference between the working electrode and the reference reversible hydrogen electrode (RHE). The inclusion of the variable U_{RHE} is how standard density functional theory (DFT) calculations of neutral interfaces are extrapolated to the electrochemical conditions of electrified interfaces.

In other words, all CHE-based approaches neglect the dependency of the interfacial structure on the applied U_{RHE}. Instead, they assume a linear dependence of free energies (ΔG) on effective U_{RHE} value:

$$\Delta G(U_{\mathrm{RHE}}) = \sum n_{\mathrm{f}} G_{\mathrm{f}} - \sum n_{\mathrm{i}} G_{\mathrm{i}} - zeU_{\mathrm{RHE}} \tag{4.6}$$

where z is the number of proton–electron transferred, $n_{\mathrm{f/i}}$ and $G_{\mathrm{f/i}}$ are amounts and free energies of the final and initial components, respectively. The subtraction of sums is the standard way of calculating a reaction energy change, where the chemical potential ($\mu_{\mathrm{H_2}}$) is substituted by the free energy of hydrogen gas ($G_{\mathrm{H_2}}$) for convenience.

Condition $\Delta G(U_{\mathrm{RHE}}) = 0$ defines the equilibrium potential ($U^{\ominus}$) of a given reaction. For HER it is 0 V, for ORR it is 1.23 V, for CO_2RR to CO it is -0.10 V, and for CO_2RR to HCOOH it is -0.11 V [20]. Depending on the electrode material, these and other reactions happen with an *overpotential* (η) – a difference between the applied electrode potential and the equilibrium potential [21]. That difference originates from the energy penalty for breaking and creating bonds at the electrode surface. In reality, it is the energy barrier for the rate-limiting step, while in the CHE-approaches, it is commonly approximated either as the energy barrier or as the difference between adsorption energies of reactive species. Both quantities describe the reaction-free energy landscape with maxima and minima corresponding to transition states and chemical species. Besides reactants and products, these chemical species include intermediates adsorbed at the catalyst's surface.

In the CHE-based approaches, the intermediates must be formed via proton-coupled electron transfer, which, on the one hand, considerably limits their choice and, on the other hand, eases their modelling. Recent reviews provide a fair and square description of coupled and separate proton and electron transfers with further details [22–25]. Let us focus on the specific example of proton-coupled electron transfer in ORR (Fig. 1).

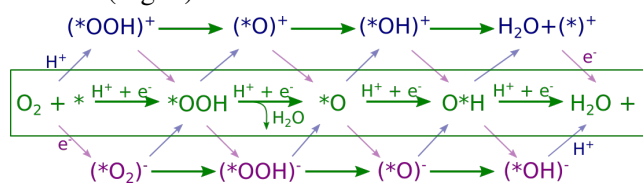

Figure 1. Illustration of variety of ORR mechanisms involving proton and electron transfers. The CHE method limits the choice to a single mechanism with proton-coupled electron transfers.

The constraint of coupling proton with electron excludes charged species, which require counter-charge in modelling with periodic boundary conditions, while molecular intermediates (O, OH, OOH) can be modelled directly using models of infinite surfaces with adsorbed radicals. Differently from the CHE-based approaches, alternative methods allow for decoupled electron transfer, like in

$O_2 + e^- \longrightarrow *O_2{}^-$, but require more complex computational techniques [26]. Note that in Fig. 1 and below, an asterisk ($*$) indicates an adsorption site on the electrode surface, and a chemical species with an asterisk (e.g., $*O_2{}^-$) stands for an adsorbate.

4.2. Computational workflows

There are two distinct approaches to modelling electrocatalytic reactions. The first approach comprehensively describes the entire electrocatalytic environment, specifically focusing on the reaction itself. The second approach breaks down the reaction into specific fragments, which are then reassembled into a general process.

Comprehensive approach. One of the objectives of computational studies is to simulate reality in order to enhance our understanding of reactions observed experimentally. This understanding requires that experiments and calculations focus on the same process under identical conditions. On the one hand, experiments should be conducted under strictly controlled conditions, using well-defined electrodes and highly pure electrolytes and reagents. On the other hand, simulations must utilise realistically sized interface models and be extended over sufficient duration to capture the atomic-level dynamics of electrochemical reactions. Conducting such detailed experiments and simulations requires an extraordinary level of effort, resulting in only a few reactions being accurately described both empirically and theoretically [27].

Fragmented approach. Rather than modelling processes as a whole, most electrocatalysis studies divide processes into elements that can be modelled with certain assumptions. These elements are then compared to distinguishable experimental features, such as limiting steps, specific effects, and structural characteristics.

For this work, we choose the common fragmentation depicted in Fig. 2: the mechanism of the reaction (involving different species and pathways), the complexity of the model system (in terms of type, size, duration, and computational methods), and the exploration of the free energy landscape (addressing both thermodynamics and kinetics). In a comprehensive approach, such as generalised CHE [8], all these are accessed simultaneously in DFT-based Molecular Dynamics. In the standard CHE-based approach, each part is approached in a step-wise workflow.

The Fig. 3 outlines our workflow used in Papers I–III. In all studies, we began with narrowing the compositional space and used Atomic Simulation Environment (ASE) as a Builder tool to create the surface of the studied catalysts, considering their composition and geometry. The next step involved using a Calculator tool to determine the formation energy of the catalyst, employing density functionals (DF), molecular mechanics (MM), or machine learning (ML). After testing various DF-based and DF tight-binding methods, MM, and several ML

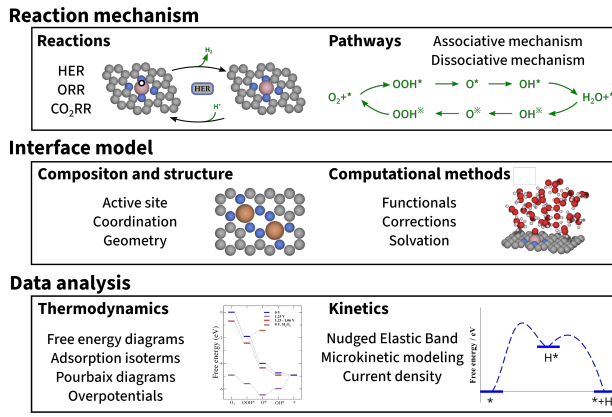

Figure 2. Fragmented approach to studying electrocatalysis with the distinction between possible products and pathways, choosing appropriate models and methods, and interpreting calculated data based on thermodynamics and kinetics.

models from the open catalyst project, we choose open source GPAW code as the Calculator tool and DFT as the Approach to predict stability and adsorption energies. To identify thermodynamically preferred reaction pathways and predict overpotentials, we used a common free energy diagram (FED). Instead of plotting a full phase diagram analysis, we compared energies of selected models, which is justified by assuming that all single atom sites are covered (as in Paper I). Instead of applying a comprehensive microkinetic analysis, we compared barriers on selected models, which is enough to account for the oxygen dissociation step (as in Paper II).

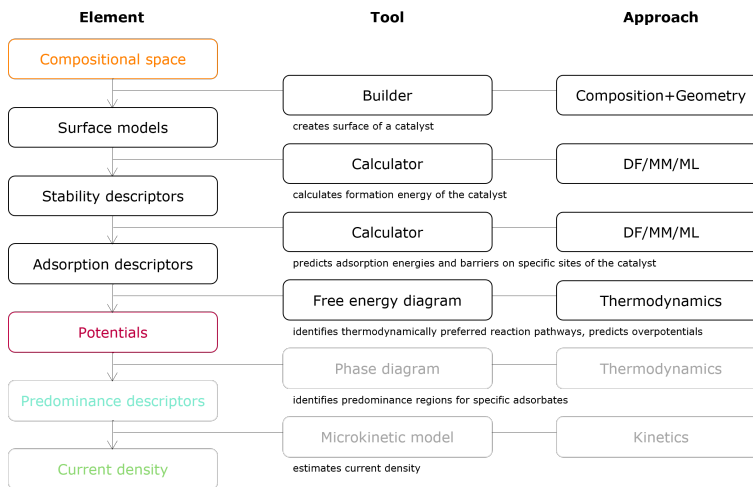

Figure 3. Diagram illustrating the workflow used in papers I–III. There are seven elements: from computational space (input) to potentials and current density (outputs). Tools enable the transition from one element to the next one by employing suitable approaches.

4.3. Atomic Simulation Environment builder

Model creation is the basic routine in computational electrochemistry. A programmable approach to building models from atoms is a good practice as it offers:

- Reproducibility of results and reduction of errors;
- Scalability to a larger number of calculations;
- Flexibility in modifying and reusing models;
- Integration with automated workflows and high-throughput calculations.

In our work, we used the ASE – an open-source package written in Python for setting up, manipulating, running, visualising, and analysing atomistic simulations [28]. From the user's perspective, the following features make ASE particularly useful as a Builder tool:

- Simple and intuitive Python interface;
- Variety functions to build atomic structures;
- Support for algorithms for molecular dynamics, structure optimisation, thermochemistry, nudged elastic band, and external calculators; simulations;
- Bayesian error estimation;
- Integrated database.

All input files for calculations in Papers I–III were written in Python using ASE functionality. For example, a Co–N–C model – a 2D periodic graphene with 4 nitrogen atoms and 1 cobalt atom – can be created in seven lines:

Listing 4.1. Creating a graphene model with 4 Nitrogen atoms and 1 Cobalt atom

```
from ase import Atom
from ase.build import graphene
MNC = graphene(size=(4,4,1))
coords = (MNC[11].position+MNC[20].position)/2
MNC.append(Atom('Co', position=coords))
[MNC[i].symbol = "N" for i in [10,13,18,21]]
del MNC[[11, 20]]
```

For calculations in Papers I–III we required build-in features of ASE: the Broyden–Fletcher–Goldfarb–Shanno algorithm [29] with a line search mechanism, vibrational analysis [30], Bayesian error estimation [31], reading and writing ASE database, nudged elastic band method [32].

In supplementary materials to Ref. [33], we provide example Python scripts for DFT optimisation and vibrational analysis along with a database for single-atom M-N-C models. FAIR data on the modelled structures, total energy values, and analysis scripts from Papers II and III are accessible on the webpages `https://nano.ku.dk/english/research/theoretical-electrocatalysis/katladb/surface-curvature-effect-on-oxygen-electrocatalysis/` and `https://nano.ku.dk/english/research/theoretical-electrocatalysis/katladb/geometry-adaptive-catalysis/`.

4.4. Density Functional Theory calculator

DFT calculations are, at present, the main approach to obtaining stability and adsorption descriptors. DFT codes with periodic boundary conditions – allowing to model surfaces as slabs – are common for the CHE-based approaches. We used GPAW code – an open-source package written in Python for electronic structure calculations. [34, 35]. GPAW and ASE are supported by large intercepting communities that provide regular updates, bug fixes, detailed documentation, and support. From the user's perspective, the following features make GPAW particularly useful as a Calculator:

- Implemented projector-augmented wave method – a well-established approach for electronic structure calculations;
- Native integration with ASE, offering a flexible and dynamic user interface;
- Support for a variety of functional from LibXC and LibvdWXC;
- Parallelization over OPENMPI and OPENMP.

For calculations in Papers I–III, we required the most basic features of GPAW, like plane-wave calculations, periodic boundary conditions, k-point sampling, and 0.9.2 pseudo-potentials. All variable parameters were tested for convergence.

Comparison of solid-state DFT codes showed a reasonable Δ-value of 1.5 meV per atom between GPAW and WIEN2k with Perdew–Burke–Ernzerhof functional (see [36]). Due to pseudo-potentials, GPAW is less precise than its commercial analogue VASP [37]. However, unlike VASP and many other codes, Python usage allows for writing inputs ASE and GPAW as a single file to execute any number of calculations and analyses in a single run. For instance, it is convenient to vary density functionals and include dispersion in tests and production runs by changing a single line of Python code.

GPAW gives access to any functional implemented in LibXC with over and LibvdWXC [38, 39]. In a preliminary methodological study, we have tested various functionals and chose the revised Perdew–Burke–Ernzerhof functional (RPBE, see [40, 41]). Foremost, among alternative functionals recommended in the literature, some are numerically ill-behaved (see [42]) and more complex functionals are computationally more demanding (such as BEEF-vdW [43]) while providing similar accuracy in predictions. RPBE is fast, robust, and shows the lowest root mean square and mean absolute deviations for prediction adsorption energies vs experimental data for chemisorption of 26 molecules [44]. In Papers I–III, we performed calculations of chemisorption. To eliminate the systematic error with CO_2, we applied a known literature correction of 0.45 eV [45, 46]. We also adapted the ASE code to perform Bayesian error estimation with RPBE (see Refs in [47]). Overall, for Papers I–III we used RPBE functional with D4 dispersion [48] correction and Bayesian error estimation [47] as a more efficient alternative to the more complex BEEF-vdW functional [43].

4.5. Technical aspects of calculations

The specific G value in the above equations can be obtained from potential energy (E) value, which is in turn calculated using DFT as well as, for example, MM [49], and ML [50]. In any case, the potential-to-free energy conversion for an adsorption state $*$A can proceed as follows:

$$G = E + \mathrm{ZPE} + \int C_P \,\mathrm{d}T - TS + \mathrm{Solv}\,, \tag{4.7}$$

where E is the DFT calculated energy, ZPE is the zero point energy correction, $\int C_P \,\mathrm{d}T$ is the enthalpy correction, TS is the entropy term, and Solv is the solvation correction.

The corrections (ZPE, entropy, enthalpy) can be applied in several ways. First, one can take them from empirical data reported in the literature. Second, they can be precisely calculated for each studied model using DFT. The second way is computationally non-trivial; thus, for high-throughput calculations, it must be well justified – meaning that the results should be clearly more improved, compared to not doing these additional calculations. In Paper I, we calculated all corrections and tested implicit and explicit solvation as in Refs. [51, 52]. In Papers II–III, we compared with intrinsic DFT errors (via Bayesian error estimation (BEE)) and noticed that the deviation from precisely calculated corrections and ones taken from previous studies is comparatively small compared to the intrinsic relative errors from DFT approach. Thus, we used the literature values for corrections [53].

By using CHE, one can calculate the adsorption energy for a given surface state $\Delta G_{*\mathrm{A}}$, as

$$\Delta G_{*\mathrm{A}} = G_{*\mathrm{A}} - G_{*} - \frac{n}{2} G_{\mathrm{H_2}}\,, \tag{4.8}$$

where n is the number of overall electrons involved in reduction (1 for $*$H, $*$COOH, $*$OCHO; and 2 for $*$CO), with $G_{\mathrm{H^+ + e^-}} = \frac{1}{2} G_{\mathrm{H_2}}$.

4.6. Free energy diagram and predicted potentials

Despite inherent limitations, the CHE successfully describes electrocatalytical processes in a variety of predictive tools, such as surface Pourbaix diagrams, adsorption isotherms, and FED [54]. The latter describes the free energy landscape along a pathway of a chosen reaction mechanism involving specific intermediates: Minima are calculated using Eq. 4.6; Maxima are estimated, for example, using the nudged elastic band (NEB) method [55–57].

In a schematic free energy diagram of ORR and OER (Fig. 4), thermodynamic minima correspond to the stable states of reactants, intermediates, and products at variable potential (U_{RHE}). The transition between two neighbouring states is a reaction step, characterised by a change in free energy and a kinetic energy

barrier – a maximum at the corresponding transition state. That diagram presents the following four steps with corresponding energy changes at $U_{\mathrm{RHE}} = 0\,\mathrm{V}$:

$$\mathrm{O_2} + * + (\mathrm{H^+} + \mathrm{e}-) \longrightarrow *\mathrm{OOH} \qquad \Delta G_1 = \Delta G_{*\mathrm{OOH}} - G_{\mathrm{O_2}} \tag{4.9}$$

$$*\mathrm{OOH} + (\mathrm{H^+} + \mathrm{e}-) \longrightarrow \mathrm{H_2O} + *\mathrm{O} \qquad \Delta G_2 = \Delta G_{*\mathrm{O}} - \Delta G_{*\mathrm{OOH}} \tag{4.10}$$

$$*\mathrm{O} + (\mathrm{H^+} + \mathrm{e}-) \longrightarrow *\mathrm{OH} \qquad \Delta G_3 = \Delta G_{*\mathrm{OH}} - \Delta G_{*\mathrm{O}} \tag{4.11}$$

$$*\mathrm{OH} + (\mathrm{H^+} + \mathrm{e}-) \longrightarrow \mathrm{H_2O} + * \qquad \Delta G_4 = -\Delta G_{*\mathrm{OH}} \tag{4.12}$$

where the adsorption free energy of $*$OH, $*$O, and $*$OOH adsorbates are defined relative to reagents and products as:

$$\Delta G_{*\mathrm{OH}} = G_{*\mathrm{OH}} - G_* - \left(G_{\mathrm{H_2O}} - \frac{1}{2}\Delta G_{\mathrm{H_2}} \right), \tag{4.13}$$

$$\Delta G_{*\mathrm{O}} = G_{*\mathrm{O}} - G_* - \left(G_{\mathrm{H_2O}} - \Delta G_{\mathrm{H_2}} \right), \tag{4.14}$$

$$\Delta G_{*\mathrm{OOH}} = G_{*\mathrm{OOH}} - G_* - \left(2G_{\mathrm{H_2O}} - \frac{3}{2}\Delta G_{\mathrm{H_2}} \right). \tag{4.15}$$

Free energy changes for each ORR step are defined by Eq. 4.6 as:

$$\begin{aligned} \Delta G_1(U_{\mathrm{RHE}}) &= -eU_{\mathrm{RHE}} + G_{*\mathrm{OOH}} - G_{\mathrm{O_2}} - G_* - \frac{1}{2}G_{\mathrm{H_2}} \\ &= -eU_{\mathrm{RHE}} + \Delta G_{*\mathrm{OOH}} - G_{\mathrm{O_2}}, \end{aligned} \tag{4.16}$$

$$\begin{aligned} \Delta G_2(U_{\mathrm{RHE}}) &= -eU_{\mathrm{RHE}} + G_{\mathrm{H_2O}} + G_{*\mathrm{O}} - G_{*\mathrm{OOH}} - \frac{1}{2}G_{\mathrm{H_2}} \\ &= -eU_{\mathrm{RHE}} + \Delta G_{*\mathrm{O}} - \Delta G_{*\mathrm{OOH}}, \end{aligned} \tag{4.17}$$

$$\begin{aligned} \Delta G_3(U_{\mathrm{RHE}}) &= -eU_{\mathrm{RHE}} + G_{*\mathrm{OH}} - G_{*\mathrm{O}} - \frac{1}{2}G_{\mathrm{H_2}} \\ &= -eU_{\mathrm{RHE}} + \Delta G_{*\mathrm{OH}} - \Delta G_{*\mathrm{O}}, \end{aligned} \tag{4.18}$$

$$\begin{aligned} \Delta G_4(U_{\mathrm{RHE}}) &= -eU_{\mathrm{RHE}} + G_{\mathrm{H_2O}} + G_* - G_{*\mathrm{OH}} - \frac{1}{2}G_{\mathrm{H_2}} \\ &= -eU_{\mathrm{RHE}} - \Delta G_{*\mathrm{OH}}\,. \end{aligned} \tag{4.19}$$

Before we discuss calculating the quantities in the above equations, let us finalise the qualitative analysis of the free energy diagram in Fig. 4. The ideal catalyst has zero free energy differences and barriers at the equilibrium potential (1.23 V for ORR). For the ideal catalyst, $\Delta G_1 = \Delta G_2 = \Delta G_3 = \Delta G_4$ and $\Delta G_{*\mathrm{OOH}} = 3\Delta G_{*\mathrm{OH}}$ with $\Delta G_{*\mathrm{O}} = 2\Delta G_{*\mathrm{OH}}$. The model catalyst has non-zero free energy differences and barriers at the equilibrium potential. For the model catalyst, all energy changes become smaller than zero (in the indicated ORR and OER directions) at overpotential values (in this example, at $\eta = 0.37\,\mathrm{V}$). The barrier values scale with the variation of free energy changes according to the Brønsted–Evans–Polanyi relation, as discussed in Sec. 6.3.2.

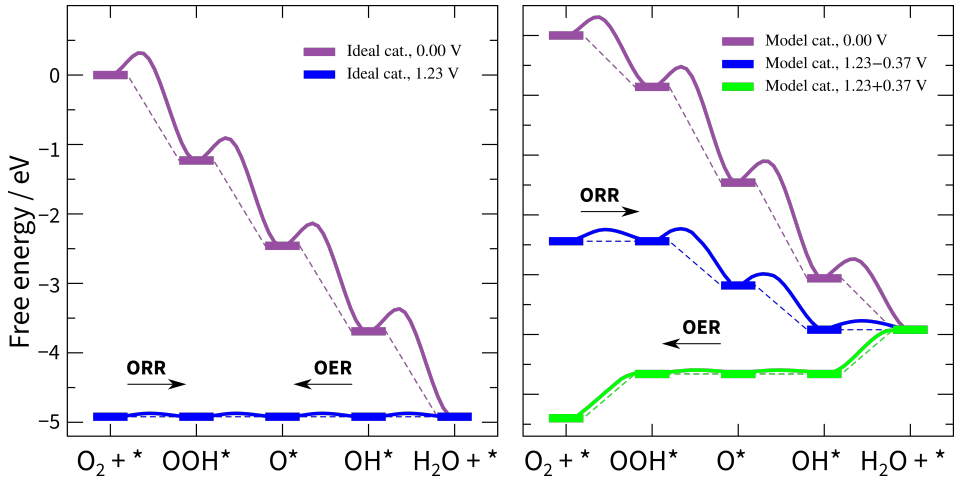

Figure 4. Free energy diagrams with thermodynamic minima and kinetic maxima at variable U_{RHE} for ideal and model catalysts.

The *limiting potential* (U_{lim}) is the lowest potential required to make all electrochemical steps downhill on the FED. For oxygen electrocatalysis, it is defined as:

$$U_{\mathrm{lim\,ORR}} = \min\left|\frac{\Delta G_i}{e}\right| \quad \text{and} \quad U_{\mathrm{lim\,OER}} = \max\left|\frac{\Delta G_i}{e}\right| \tag{4.20}$$

where $|\Delta G_i|$ is the absolute value of the change in free energy for the i-th reaction step – either minimum for ORR or maximum for OER (see Fig. 4).

U_{lim} is most useful for reactions with variable products, like CO_2RR. In the case of simpler oxygen electrocatalysis, overpotential is commonly used to describe catalysts' activity as:

$$\eta_{\mathrm{ORR}} = U^{\ominus} - U_{\mathrm{lim\,ORR}} \quad \text{and} \quad \eta_{\mathrm{OER}} = U_{\mathrm{lim\,OER}} - U^{\ominus} \tag{4.21}$$

5. STRUCTURAL EFFECT IN CARBON DIOXIDE ELECTROREDUCTION

This chapter is about selectivity in electrocatalysis and wishful thinking in research. Let us first elaborate on the last component. Wishful thinking is common in electrocatalysis in the form of attributing the ability to catalyze specific reactions to certain elements. For example, it is known that metallic copper catalyzes C_2^+ reduction of CO_2. On that basis, many researchers focus on various compounds of copper, some of which do show high activity at first sight [58]. However, under closer inspection, it turns out that it is still metallic copper formed in preparation. For example, some works report Cu-N-C materials as good catalysts [58, 59], yet one work questions this conclusion simply by showing the formation of copper nanoparticles from Cu-N-C during operation [60]. Similarly, the motivation of my colleagues was extrapolating the exceptional selectivity of metallic bismuth to Bi-N-C in catalysing CO_2 reduction to HCOOH in Paper I. However, the computational modelling predicted that bismuth nanoparticles are responsible for selectivity, whether Bi-N-C remains relatively inactive spectator.

5.1. Literature overview

The valorization of CO_2 is an ongoing effort to mitigate climate change. The necessity is evident by the wide range of recently emerging carbon capture and storage (CCS), and carbon capture and utilisation (CCU) technologies [61–63]. In particular, a contrast must be made between the *utilisation* and *storage* part, meaning that the CO_2 is not only stored and kept away from reentering the atmosphere (thus, *stored*) but used and reused to yield valuable products (thus, *utilised*) [64, 65].

Of significant importance in CCU is the CO_2 electroreduction, enabling the use of renewable energy to yield a range of valuable fuels, hydrocarbons, and other highly desired C-compounds in a net carbon-neutral way [66–68]. While the range of the possible products is vast, it also means that certain problems arise when considering the selectivity of the electrocatalysts. Thus, to simplify the problem, certain rules of thumb have been formulated based on experimental measurements and computational predictions [69]. In general, the selectivity of CO_2 electroreduction can be divided into three major categories: (1) reduction to carbon monoxide, (2) reduction to formic acid, and (3) reduction beyond carbon monoxide (methanol, methane, ethanol, etc.) [19]. To make matters worse, not only do the (good) electrocatalysts have to be highly selective towards the wanted product, but also the parasitic HER has to be sufficiently disfavoured to obtain acceptable electrocatalytic efficiency [70, 71]. As the space of possible products and electrocatalysts is surprisingly large, computational modelling is a necessary part of developing CO_2 electroreduction.

The DFT modelling has been successfully applied to CO_2 electroreduction to predict and/or explain the activity [72–74]. In this context, we highlight the key CO_2 electroreduction pathways to carbon monoxide and formic acid. Let us note that the CO pathway under specific circumstances (notably, on copper-based catalysts) can continue to other C_1 products, such as formaldehyde, methanol or methane, or even C_{2+} products, such as ethanol, ethane or others [75–77].

In Paper I, we applied computational modelling to explain the structural effect on carbon dioxide electroreduction by considering two of the key pathways on common moieties found in carbonised catalysts – metal–nitrogen–carbon (M–N–C) species and metal nanoparticles (NPs). Specifically, the effect is shown on metal-organic framework (MOF)-derived catalyst pyrolysed at several temperatures, allowing the observation of various structural changes with experimental and computational methods.

5.2. Structural models

Pyrolysis-derived catalysts contain a variety of NPs and M–N–C species [78, 79]. To model key structures present in these catalysts, several structures were constructed and optimised. The calculations were performed for 2D-periodic slabs with at least 14 Å vacuum layer in a non-periodic direction, using 2×2×1 Monkhorst–Pack k-point sampling.

Metal nanoparticle modelling. To represent the surface of bismuth NPs, the Bi(111) facet was used due to it being the most common cleavage plane and the stablest Bi facet [80–82]. For Bi(111) models, a 3×3×4 supercell was used, with the two bottom layers constrained thorough the calculations. The supercell size was chosen to balance the avoidance interaction between modelled adsorbates yet keep the calculations reasonably fast.

M–N–C modelling. To represent Bi-N-C moieties in the M–N–C active sites, three models were constructed: (1) BiN_4 embedded in graphene layer, (2) BiN_2C_2 site embedded in graphene layer with nitrogen in *cis* positions, and (3) BiN_2C_2 site embedded in graphene layer with nitrogen in the *trans* positions. For all three structures, the model was constructed from a 3×3×1 graphene supercell, and the active sites were introduced by replacing up to 6 carbon atoms in the structure (as described in Sec. 4.3).

Adsorbates. The models were combined with adsorbates, denoted as ∗Ads, to obtain information about the relevant CO_2 reduction pathways to CO (∗COOH, bound to surface via C atom, and ∗CO intermediates) and HCOOH (∗OCHO, bound to surface via O atom, intermediate). In addition, the competing HER pathway was considered (∗H intermediate).

Pathways. The electrochemical reactions considered are as follows:
CO pathway:

$$* + CO_2 + H^+ + e^- \longrightarrow *COOH, \tag{5.1}$$
$$*COOH + H^+ + e^- \longrightarrow *CO + H_2O, \tag{5.2}$$
$$*CO \longrightarrow * + CO. \tag{5.3}$$

HCOOH pathway:

$$* + CO_2 + H^+ + e^- \longrightarrow *OCHO, \tag{5.4}$$
$$*OCHO + H^+ + e^- \longrightarrow * + HCOOH. \tag{5.5}$$

HER pathway:

$$* + H^+ + e^- \longrightarrow *H, \tag{5.6}$$
$$*H + H^+ + e^- \longrightarrow * + H_2. \tag{5.7}$$

5.3. Results and discussion

Computational results. The DFT calculation results are given in the Table 1 and predicted U_{lim} are summarised in Fig. 5. The following facts can be observed: (1) In all cases CO pathway is less favourable than HCOOH pathway ($U_{\text{lim HCOOH}} < U_{\text{lim CO}}$). (2) The HCOOH pathway is the most favourable (the lowest U_{lim}) on BiN_2C_2-*cis* structure. However, when comparing the absolute energies of BiN_2C_2-*cis* and BiN_2C_2-*trans* structures (that are isoelectronic), BiN_2C_2-*trans* turns out to be more stable, thus, more likely to be formed. (3) Bi(111) is more selective towards formic acid (higher ΔU_{lim}) and active (lower U_{lim}).

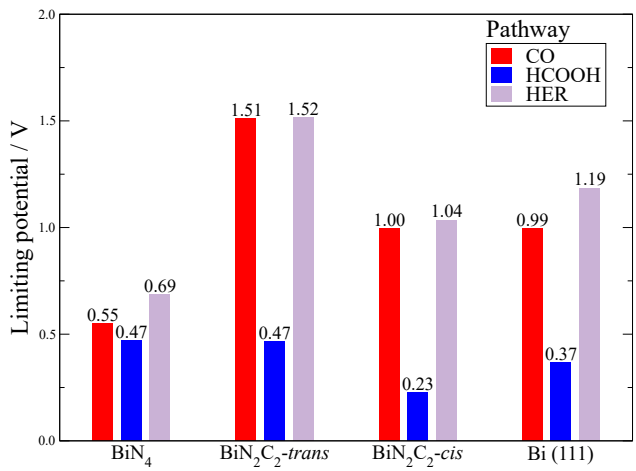

Figure 5. Limiting potentials for CO_2 reduction on bismuth surfaces.

To further analyse the data, we need to consider FED, which are shown in Fig. 6. FED provide additional insights: (1) BiN_4 binds both ∗COOH and ∗OCHO intermediates stronger. Interestingly, this causes the CO pathway to become more favourable, but HCOOH pathway less favourable – explaining the significant drop in the ΔU_{lim} and, therefore, lower selectivity when compared to Bi(111). (2) The strong adsorption of ∗OCHO intermediate on BiN_4 could, over time, poison the active sites as the second reduction step to yield HCOOH has a comparably higher reaction barrier.

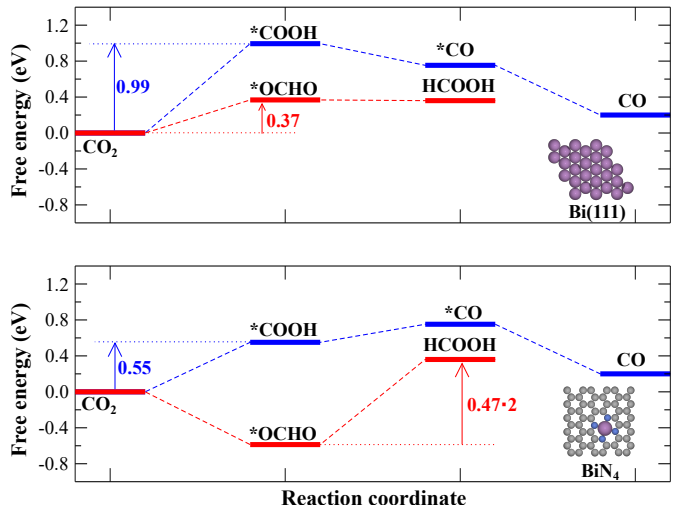

Figure 6. Free energy diagrams for CO_2 reduction at Bi(111) and BiN_4 model surfaces.

Table 1. Table of DFT calculated adsorption energies (in eV) for all relevant species. A comparison data is added for the corrections with previously used literature values [83].

Species	$E_{*\mathrm{A}}$	ZPE	$\int C_P \mathrm{d}T$	TS	Solv	$G_{*\mathrm{A}}$
BiN_4	-523.84	0	0	0	0	-523.84
BiN_2C_2-*trans*	-524.32	0	0	0	0	-524.32
BiN_2C_2-*cis*	-524.21	0	0	0	0	-524.21
Bi(111)	-168.10	0	0	0	0	-168.10
BiN_4–COOH	-550.00	0.63	0.09	0.15	-0.30	-549.73
BiN_2C_2-*trans*–COOH	-549.46	0.61	0.10	0.20	-0.30	-549.25
BiN_2C_2-*cis*–COOH	-549.95	0.65	0.08	0.13	-0.30	-549.65
Bi(111)–COOH	-193.75	0.61	0.10	0.21	-0.30	-193.54
lit. comparison		0.62	0.10	0.18		
BiN_4–OCHO	-551.48	0.67	0.07	0.12	0.00	-550.87
BiN_2C_2-*trans*–OCHO	-550.37	0.64	0.09	0.18	0.00	-549.82
BiN_2C_2-*cis*–OCHO	-550.99	0.64	0.09	0.16	0.00	-550.42
Bi(111)–OCHO	-194.73	0.65	0.09	0.18	0.00	-194.17
lit. comparison		0.62	0.10	0.23		
BiN_4–CO	-538.83	0.18	0.08	0.16	0.00	-538.73
BiN_2C_2-*trans*–CO	-539.31	0.18	0.09	0.19	0.00	-539.23
BiN_2C_2-*cis*–CO	-539.16	0.22	0.06	0.12	0.00	-538.99
Bi(111)–CO	-183.15	0.21	0.06	0.11	0.00	-182.98
lit. comparison		0.19	0.08	0.15		
BiN_4–H	-526.68	0.15	0.01	0.02	0.00	-526.54
BiN_2C_2-*trans*–H	-526.35	0.17	0.01	0.01	0.00	-526.19
BiN_2C_2-*cis*–H	-526.71	0.17	0.01	0.02	0.00	-526.56
Bi(111)–H	-170.42	0.15	0.02	0.02	0.00	-170.30
lit. comparison		0.16	0.01	0.01		

Comparison to experimental data. The computational data explains the experimental observations of CO_2RR behaviour on three differently prepared bismuth MOF-derived catalysts. The relevant summary of experimental results is given in Table 2. Here, we can note the following: (1) TAL−33−400 experiences a significant drop in Faradaic efficiency in 4 hours, which can be attributed to the very high presence of Metal-N_x species (in computational modelling corresponding to Bi-N-C surfaces), consistent with the strong binding of ∗OCHO intermediate on BiN_4 surface. (2) The best selectivity (Faradaic efficiency) is observed for the catalyst with the highest metal to Metal-N_x ratio. Consistent with the computational results that Bi(111) has the highest selectivity towards HCOOH.

Table 2. Summary (for full data and experimental conditions refer to Paper I) of experimental data for bismuth MOF-derived catalyst. $FE_{initial}$ – Initial Faradaic efficiency for HCOOH formation, $FE_{4\ hours}$ – Faradaic efficiency after chronoamperometry measurements at −1.0 V vs RHE for 4 hours, Surf. Bi – Bismuth surface content as measured by XPS, Metal-N_x content as measured by XPS.

Designation	$FE_{initial}$ / %	$FE_{4\ hours}$ / %	Surf. Bi / at%	Metal-N_x / %
TAL−33−400	90	52	2.6	33.7
TAL−33−500	95	93	2.3	17.0
TAL−33−600	98	94	2.4	7.6

5.3.1. Summary and perspectives

The studied structural effect clarifies the selectivity observed in bismuth MOF-derived catalysts. Computational modelling demonstrates that a higher mass content ratio of bismuth NPs compared to M-N-C species results in greater HCOOH selectivity. This finding underscores the importance of accurately identifying active sites and understanding structural effects in electrocatalysts. It also highlights the pitfalls of wishful thinking in research, where assumptions about catalytic abilities based on elemental properties can lead to incorrect conclusions. The study emphasises the critical role of computational modelling as a method for predicting and explaining effects, ensuring more reliable and effective catalyst development.

6. SURFACE CURVATURE EFFECT IN OXYGEN ELECTROCATALYSIS

6.1. Literature overview

6.1.1. Oxygen electrocatalysis

Oxygen electrocatalysis, including ORR and OER, is an important set of electrochemical reactions required for electrochemical energy storage and conversion (ESC) devices [84, 85].

The benchmark catalysts in oxygen electrocatalysis are based on platinum group metals (PGMs), namely, for ORR, it is Pt, while for OER, it is IrO_2 or RuO_2 [86, 87]. The associated problems, such as low abundance and high costs, with PGMs use are well recognised, leading to a significant amount of research in alternatives [88, 89]. In particular, M–N–C are of great interest, providing significantly better atom utilisation due to the single atom sites (SASs), and much higher abundance of the commonly used metals, Fe, Ni, Mn, and other first-row transition group metals [90–94].

From a theoretical perspective, oxygen electrocatalysis is interesting due to its $4e^-$ mechanism with non-trivial thermodynamics and well-established limitation – scaling relations [95–99]. As it is fundamentally important to understand and consider what is scaling relations and how they can be dealt with, the next subsection will focus on it in more detail.

6.1.2. Scaling relations

Mechanisms. To begin the discussion about scaling relations, we must introduce the relevant mechanisms. The most prevalent and most studied oxygen electrocatalysis mechanism is *associative mechanism*, occurring on SASs, for which the elementary steps are shown in Eq. 4.9. In contrast, on dual atom sites (DASs), another common type of mechanism, *dissociative mechanism*, is possible:

$$2* + O_2 + H^+ + e^- \longrightarrow *O + *OH, \tag{6.1}$$

$$*O + *OH + H^+ + e^- \longrightarrow *OH + *OH \tag{6.2}$$

$$\text{or} \quad *O + *OH + H^+ + e^- \longrightarrow *O + * + H_2O \tag{6.3}$$

$$*OH + *OH + H^+ + e^- \longrightarrow *OH + * + H_2O, \tag{6.4}$$

$$\text{or} \quad *O + * + H^+ + e^- \longrightarrow *OH + * \tag{6.5}$$

$$*OH + * + H^+ + e^- \longrightarrow 2* + H_2O. \tag{6.6}$$

While other possible mechanisms exist and can be found in the literature [100, 101], the aforementioned two form the best basis for our further discussion and are consistent with the models considered later in the dissertation. First, because there is a limited set of how adsorbates can transform into one-another *via* proton-

coupled electron transfer. Second, because these intermediates are observed by characterisation techniques in experiment [102].

Scaling relations. In general, the adsorption energies of different adsorbates, A and B, on the same catalyst are correlated *via* the expression

$$\Delta G_{\mathrm{A}} = \alpha_{\mathrm{A,B}} \cdot \Delta G_{\mathrm{B}} + \beta_{\mathrm{A,B}}\,, \tag{6.7}$$

where the α is the slope and β is the intercept for a given scaling relation. The literature offers an explanation for the origin of these parameters; namely, the slope is determined by the number of bonds between the adsorbate and the surface (commonly referred to as electron counting rules), while the intercept has a more complex origin, including neighbouring coordination numbers and nature of the active site, approximately following a dependence also on the slope, as

$$\beta_{\mathrm{A,B}} = \alpha_{\mathrm{A,B}}\beta_1 + \beta_2\,. \tag{6.8}$$

In relation to oxygen electrocatalysis, two scaling relations play an important role in describing (and limiting) the activity, shown in Fig. 7. First, the most well-known one links the associative intermediates $*$OOH and $*$OH so that

$$\Delta G_{*\mathrm{OOH}} = 1 \cdot \Delta G_{*\mathrm{OH}} + 3.2 \pm 0.2\,. \tag{6.9}$$

The slope is close to 1 due to the hydroxide and peroxide adsorbates, both of which are of single-bond character, thus consistent with electron-counting rules. The intercept can be explained in two ways:

1. A standard explanation relates the β value to the free energy difference between HO_2^- and HO^- in an aqueous solution. This difference can be estimated from the equilibrium potential and dissociation constants as $\beta \approx [4 \cdot 1.23 - 2 \cdot 0.69 + 0.059 \cdot (11.6 - 14.0)] \approx 3.4\,\mathrm{eV}$.
2. An alternative estimation can be obtained by considering Eq. 6.8, as the slope is 1, it can be simplified to $\beta = \beta_1 + \beta_2$. Here, β_2 is the free energy of formation for H_2 and H_2O (2.46 eV) and β_1 is the difference in going from double bond in O_2 to single-bond in $*$OOH. This value can be derived from the difference in bond dissociation energy values (from literature values of O_2, H_2O, and CH_3CO_3H the estimated range for β_1 is from 0.40 to 0.84 eV). Thus, (without considering additional contributions from bonding and solvation) the estimate for intercept is $\beta \approx 3.1 \pm 0.2\,\mathrm{eV}$.

A more contentious one is linking $*$O and $*$OH intermediates, so that

$$\Delta G_{*\mathrm{O}} = 2 \cdot \Delta G_{*\mathrm{OH}} + 0.5 \pm 0.7\,. \tag{6.10}$$

The explanation for slope is as follows from electron counting rules, and considering that $*$O has a double bond, while $*$OH has a single bond to active site, thus clearly the expected value is around 2. For the intercept, the estimated value is $\beta \approx 0.5 \pm 0.7\,\mathrm{eV}$, agreeing with the fit shown in Fig. 7.

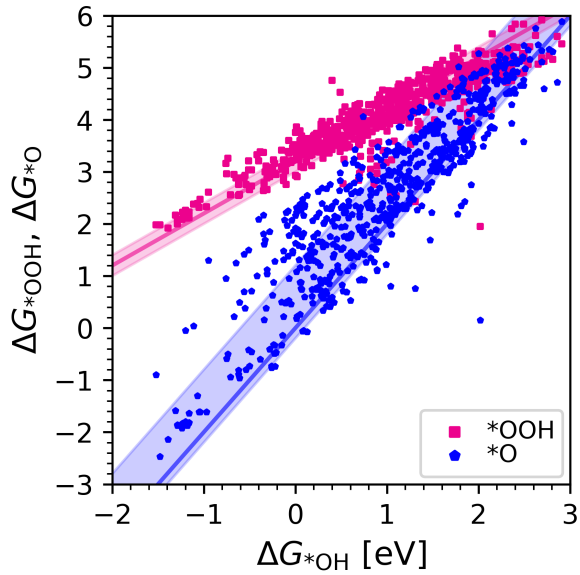

Figure 7. Scaling relations for key oxygen reduction intermediates, ∗OOH and ∗O vs ∗OH. The solid lines illustrate the commonly accepted slopes and intercepts, while the shaded region indicates spread in Eqs 6.9 and 6.10. Adsorption energies taken from the literature [96, 103].

Similarly, we can also consider the scaling for dissociative mechanism (using the shorthand ∗O/OH to describe DASs with ∗O + ∗OH):

$$\Delta G_{*\mathrm{O/OH}} = 3 \cdot \Delta G_{*\mathrm{OH}} + 0.5 \pm 0.7\,, \tag{6.11}$$

where the slope of 3 corresponds to the 3 bonds (2 from ∗O and 1 from ∗OH), while the intercept is from sterical repulsion between the adsorbed on the active sites.

6.2. Surface curvature effect

6.2.1. Flat or curved?

In computational modelling mostly all materials are considered as flat surfaces. To give an example, we can consider the vast research on metal surfaces [104], reviews on the development and screening of M–N–C catalysts [53], studies on MX-enes [105], or many others [106, 107]. Case in point, the models discussed in the previous Sec. 5 are all flat 2D structures with periodicity in two dimensions. The *flatness* of models is highly convenient and, in a lot of cases, sufficiently captures the main governing effects of catalytic activity. Nevertheless, as catalyst design evolves to meet the increasing need for more and more active (and stable) materials, the edge cases where subtle effects that distinguish *curved* catalysts from *flat* ones become increasingly more interesting.

A minireview [108] published in 2021 highlights that "Recently, scientists found that the surface curvature of electrocatalysts could play an important role for the improvement of catalytic performance and the optimisation of intrinsic catalytic activity during electrocatalytic process". In some way, this is surprising, as surface curvature is an intrinsic property of many catalysts and, therefore, should have become an essential consideration a long time ago. The unexplored nature becomes more apparent when one considers the difficulties of modelling the curvature in comparison to flat catalysts. In particular, introducing curvature in the models changes the periodicity (or requires unwieldy large models to represent the curvature periodically), which widely differs from the classical slab models standard in electrocatalysis [109]. The specific details on introducing curvature in models depend on the type of catalyst, and further, the discussion is limited to M–N–C catalysts.

Even within M–N–C catalysts, the curvature can arise in different ways. One of the first models in the context of M–N–C catalysts that were investigated for curvature were carbon nanotubes (CNTs) [110–112]. One of the reasons why that is the case is that this simplifies the modelling because CNTs can be represented as molecules or straightforward 1D systems. The limitation of focusing on only CNTs is twofold; first, the system size significantly depends on the size of CNTs, and so, for large curvatures, the model gets prohibitively large, and second, the CNTs does not allow modelling concave curvature, commonly observed in amorphous catalysts [113]. In contrast, the modelling of general M–N–C catalyst is rather different, and in literature, has been achieved via modelling strain effect [114, 115].

6.2.2. Effect of curvature

In general, we can distinguish two ways the curvature can affect a catalyst compared to a reference of *flat* catalyst. These two effects to be discussed are not unique to curvature and apply to all catalysts, yet note that curvature allows modifying them more incrementally compared to alternatives (e.g. change of structure).

Geometric effect. This effect reflects the geometric changes in structure due to a change in curvature. With respect to oxygen electrocatalysis, this can correspond to a change in active site proximity, thus enabling the alternative pathways (e.g. switch from the associative pathway to the dissociative one).

Electronic effect. This effect reflects the chemical changes due to atoms being differently coordinated within a structure due to a change in curvature. The resulting change in the chemical environment thus causes changes in the, for example, electronic structure, which is highly correlated to the adsorption energies of oxygen intermediates.

In general, both of these are important (and highly coupled), and thus, to explore both effects in more detail, let us consider the dual-site M–N–C model for oxygen electrocatalysis.

6.2.3. Modelling surface curvature effect

Model considerations. A typical M–N–C model can be constructed from a graphene supercell by replacing 6 of the carbon atoms in the supercell with MeN_4 site, as, for example, described in Sec. 5.2. However, to introduce curvature, a 2D graphene supercell can be replaced with a nanoribbon that is periodic only in one direction (similar to CNTs). When it comes to nanoribbons, several possible structures are possible and have been studied for oxygen electrocatalysis. Nevertheless, in this case, we focus on specific general M–N–C model properties, and nanoribbon hydrogens serve only to cap the non-periodic direction. Therefore, specific considerations should be taken into account so that the constructed model resembles a regular M–N–C model system. This is achieved via a sufficient number of carbon atoms along the non-periodic carbon plane so that resulting MeN_4 sites do not interact with the capping atoms significantly. Additionally, the armchair nanoribbon is chosen as it provides convenient symmetry.

Introducing curvature. Given that we have a model with one non-periodic direction that we can adjust, the curvature can be introduced by considering a line in the graphene plane perpendicular to the axis of the periodic direction. Using a coordinate transformation, this line can be mapped to a circle with a selected radius r, and accordingly, the atom positions can be moved to correspond to the new coordinates – resulting in a curved plane of atoms with a specific curvature radius. Afterwards, the created structure is optimised by keeping selected edge atoms constrained to keep the curvature yet allow the overall structure to relax. As it is observed from the calculations, the resulting optimisation doesn't significantly change the introduced curvature.

Oxygen electrocatalysis considerations. As the main focus of the surface curvature effect, as studied here, is oxygen electrocatalysis, a specific choice of the introduced metal sites must be taken. Accordingly, using previous literature knowledge, it seemed interesting to consider two models with (1) two CoN_4 sites and (2) one CoN_4 site and NiN_4 site. To explain this choice, CoN_4 sites are conveniently close to ideal adsorption energy for $*OH$ intermediate, and NiN_4 sites have lower oxygen affinity (higher adsorption energy), and thus a more clear picture of the secondary effects from the secondary site can be identified. This leads to a model for the surface curvature effect, where the curvature is induced by changing the curvature radius.

Model specific considerations. The model with the variable curvature radius r (thus fixing also angle θ and metal atom distance d_r) is shown in Fig. 8. The descriptor for *geometric effect* is the metal atom distance; therefore, it is important to relate this distance with the curvature. Let us consider the distance between metal centres in the planar configuration as d_∞ and the metal atom distance at pore radius r (and thus specific curvature) as d_r. d_r can be expressed in terms of r and θ to yield

$$d_r = 2r\sin(\theta)\,. \tag{6.12}$$

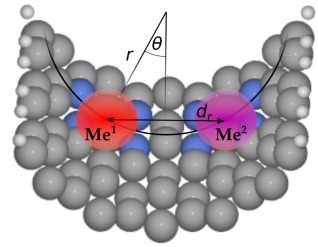

Figure 8. Computational model for surface curvature effect studies with the relevant variables.

The chord of the marked circle corresponds to d_∞ and therefore in terms of r and θ, we have that

$$d_\infty = \frac{2\theta}{2\pi} \cdot 2\pi r = 2\theta r\,. \tag{6.13}$$

We can solve for θ, so that $\theta = \dfrac{d_\infty}{2r}$ and insert in Eq. 6.12:

$$d_r = 2r\sin\left(\frac{d_\infty}{2r}\right) = \frac{d_\infty}{d_\infty} \cdot 2r\sin\left(\frac{d_\infty}{2r}\right) = d_\infty\,\mathrm{sinc}\left(\frac{d_\infty}{2r}\right). \tag{6.14}$$

However, since only a certain range of r makes physical sense (corresponding to experimentally observable curvatures with the possibility to accommodate adsorbates, thus $r > 3$ Å), we can apply Taylor expansion to the Eq. 6.14 so that

$$d_r = d_\infty - \frac{d_\infty^3}{24} \cdot \frac{1}{r^2}\,. \tag{6.15}$$

We can visually verify the approximation, as shown in Fig. 9. To obtain appropriate spacing in the linearization with respect to $\frac{1}{r^2}$, models with curvatures of ∞ (flat model, reference state), 8.5, 8.0, 6.0, 4.0 Å were created and further optimised.

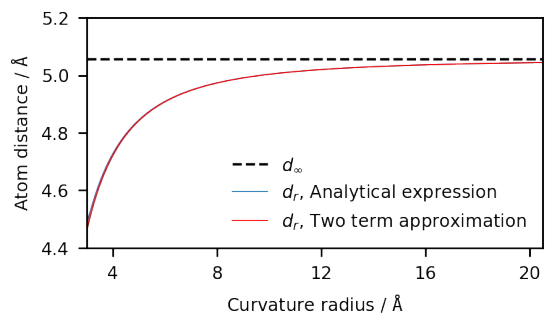

Figure 9. Inter-site distance d_r dependence on the curvature radius r.

6.2.4. Results of surface curvature effect

Effect on adsorption energies. The primary question with regards to the surface curvature effect is, "How does the curvature affect adsorption energies?". The effect of surface curvature on oxygen electrocatalysis intermediates is shown in Fig. 10. We can understand the results by considering both *electronic effect* from the curvature and *geometric effect*, as described above. First, for the *electronic effect* we can observe that the adsorption energies increase with the curvature. From an electronic perspective, it is attributed to the fact that inducing curvature changes the electronic structure of the active site and, therefore, destabilises the intermediate adsorption. Furthermore, noticeable is also the fact that for dissociative intermediates, the slope is steeper than that of associative intermediates. This is an obvious result, as we destabilise the adsorbates on two sites for a dissociative mechanism in comparison to a single site in the associative mechanism. Nevertheless, an interesting feature is that for the dissociative mechanism on the $2\times CoN_4$ model, the dissociative $*O/OH$ adsorption intermediate fit line crosses the ideal adsorption energy for that intermediate. This leads to a broader interest in the *geometric effect* and the possibilities of switching the mechanism from associative to dissociative.

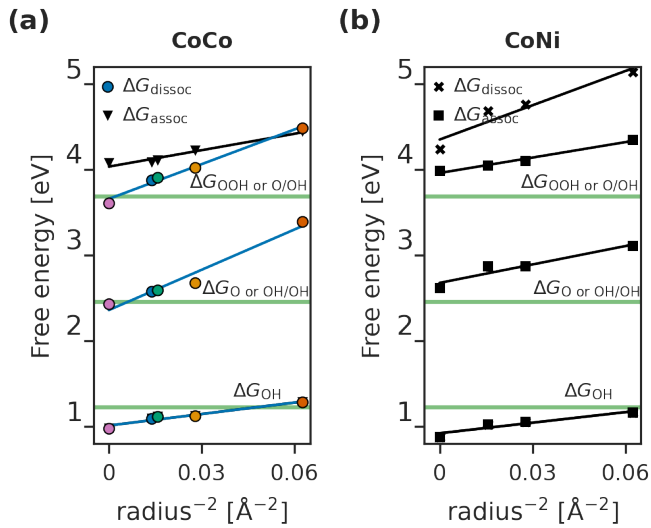

Figure 10. Effect of curvature radius r on the adsorption energies. The green lines indicate the ideal adsorption energy for the given adsorbate.

We find that surface curvature affects adsorption energies with a linear dependence on the inter-atomic distance of the active sites. For significant arising results from that, we will return in Sec. 6.3. For now, let us consider the implications of surface curvature on oxygen electrocatalysis in the context of overpotential volcanoes.

Effect on overpotential volcano. The overpotential volcano is a convenient tool to easily inspect and correlate the adsorption energies to overpotential for oxygen electrocatalysis. The results for the present study are shown in Fig. 11, from which we can immediately draw several interesting results. Namely, that:

- For both 2×CoN_4 and $CoN_4 + NiN_4$, the associative mechanism energies closely follow the classical scaling relation. Yet it allows fine-tuning the energy along the scaling relations.
- A more interesting behaviour is observed for the dissociative mechanism adsorption energies. The dissociative mechanism nicely shows different scaling relations; we can discuss the slope and intercept in some detail.

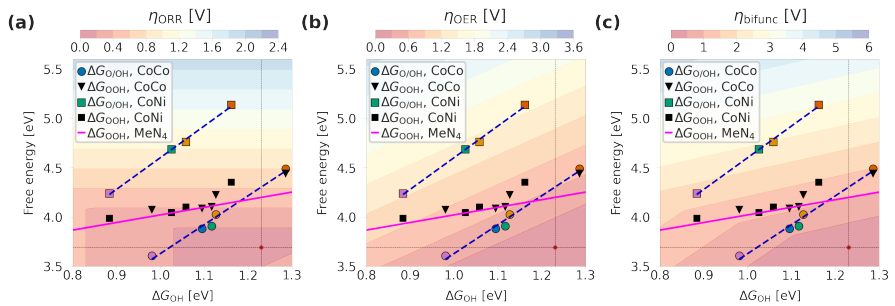

Figure 11. Overpotential volcanoes for (a) ORR, (b) OER, and (c) bifunctional oxygen electrocatalysis. Markers identify the structures calculated in the present study, while the magenta fit line is used to show the literature data for a general MeN_4 active site.

Nevertheless, even though the overpotential volcano is a nice rule-of-thumb and allows the filtering of the most promising structures, a full analysis in the form of a FED is needed to precisely determine overpotentials (as the scaling relations are not holding 100% strictly).

Effect on FED. To obtain a full thermodynamic picture of oxygen electrocatalysis, FEDs were constructed for the dissociative mechanism on the 2×CoN_4 model, as shown in Fig. 12. The main difference from the overpotential volcano picture is that FEDs consider the exact energies instead of using the scaling relation approximation ($\Delta G_O \approx 2 \cdot \Delta G_{OH}$) that are used to construct volcanoes. Thus, an interesting feature arising from considering the full FED picture is that the predicted bifunctional overpotential (0.45 V) is noticeably lower than that predicted just by the overpotential volcano picture (≈0.7 V). Nevertheless, even the FED does not capture all the aspects of oxygen electrocatalysis. In reality, the dissociative mechanism can instead be limited by the dissociation of O_2, which is not an electrochemical step. To explore the possibility of splitting O_2, NEB analyses were performed to obtain an estimate for the kinetics of dissociation.

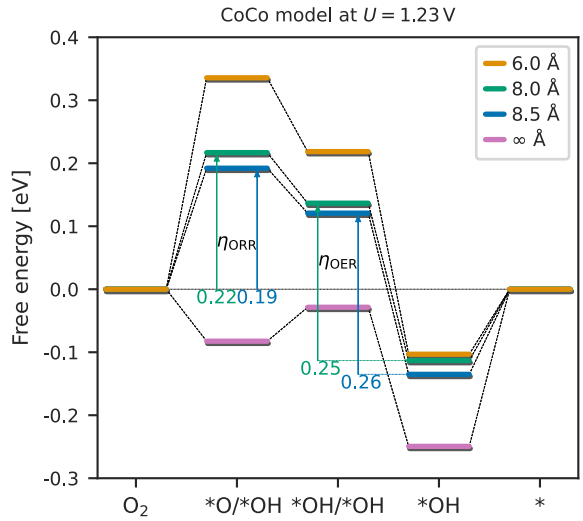

Figure 12. FED at oxygen reduction and evolution equilibrium potential for 2×CoN_4 model with dissociative mechanism.

Geometric effect and NEB. Up to now, we have stated that the *geometric effect* of surface curvature can bring the two sites closer together and thus induce the switch to a dissociative mechanism. The *geometric effect* of the switching can be quantified by a descriptor – here, we use the energy barrier as obtained from NEB to switch from ∗OOH intermediate to ∗O/OH intermediate. The energy changes along the reaction coordinate when switching between these intermediates are shown in Fig. 13. The peak of the interpolated free energy approximates the dissociation barrier needed to switch the mechanisms.

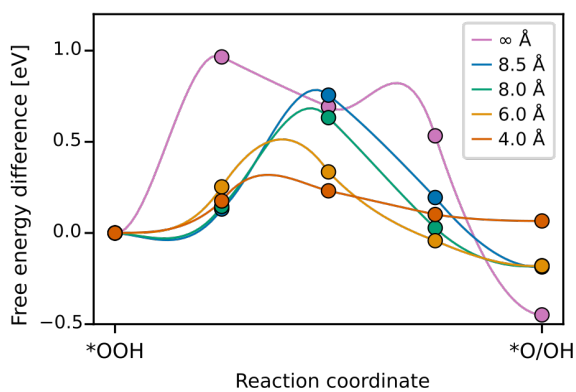

Figure 13. Nudged elastic band calculations for the oxygen dissociation.

An interesting comparison can be made between the dissociation barrier (kinetic effect) versus the obtained gain with respect to scaling relations ($G_{O/OH} - G_{OOH}$, thermodynamic effect). These results are summarised in the Table 3. With

the aid of this table, we can clearly distinguish the *geometric effect* with the decrease in dissociation barrier G_a as the curvature increases, and *electronic effect* with the change of intermediate adsorption energy difference changing.

Table 3. NEB calculation results contrasted with the change in adsorption energies for dissociative and associative intermediates. More negative $G_{O/OH} - G_{OOH}$ indicates more favourable dissociative mechanism, while smaller G_a indicates more favourable dissociation barrier.

r / Å	G_a / eV	$G_{O/OH} - G_{OOH}$ / eV
∞	0.97	−0.45
8.5	0.78	−0.19
8.0	0.68	−0.18
6.0	0.51	−0.18
4.0	0.32	0.07

6.2.5. Summary and perspectives

The surface curvature effect on M–N–C catalysts affects the adsorption energies (via the change in electronic structure – *electronic effect*) and the reaction pathway (via the change in the intersite distance – *geometric effect*).

In relation to oxygen electrocatalysis, this means that a curved M–N–C catalyst can bring two active sites close enough to enable the dissociative pathway and, therefore, break the scaling relations leading closer to the apex of the overpotential volcano at the same time further increasing the bifunctional activity. The surface curvature effect further allows to fine-tune the dissociative mechanism intermediate adsorption energies to optimise the overpotential for the given mechanism.

Additionally, of particular importance is the finding that the adsorption energies are linearly changing with the curvature. This leads to fascinating predictions in the context of dynamic catalysts, as we will discuss in the next section.

We can also imagine the perspectives that the surface curvature could apply to the discussion in Sec. 5. Particularly, the *electronic effect* part of the surface curvature effect could be used to raise the adsorption energy of ∗OCHO intermediate, thus reducing the U_{lim} for the limiting step of ∗OCHO reduction to formate. However, the application requires a few more considerations that have not been researched; for example, how would the other pathway intermediates, ∗H and ∗COOH, be affected by the curvature? Here, only the adsorbates that bind to the surface via oxygen atoms have been considered, yet from a theoretical perspective, the behaviour of adsorbing via carbon or hydrogen can result in different dependence (and magnitude) of the change in adsorption energy with curvature.

6.3. Geometry adaptive catalysts

6.3.1. Static or geometry adaptive?

The structure of catalysts is always in thermal motion. The atoms translate, rotate, and vibrate. The speed of these motions is comparable to catalytic turnover frequencies. In computations, a general focus is on stable, thermodynamic minima. The adsorbate kinetics in reactions are also considered important. The structural changes of the catalyst during the reaction are less explored.

A common strategy in electrocatalysis for observing interesting phenomena is by referring to nature citebarrioBioinspiredBioderivedAqueous2023. The phenomena of structural changes during catalysis is no exception. A well-known reference molecule is cytochrome *c* oxidase (CcO), inspiring many research directions in an attempt to mimic its activity [116]. Notably, looking closely at the mechanism explaining the CcO activity, one can observe a change in Fe–Cu distance during the reaction, which is a sign of geometry adaption.

To note examples of *artificial catalysts* where geometry adaption has been shown to play an important role, we can refer to platinum nanoclusters [117]. Sufficiently small Pt-nanoparticles are highly dynamic and, during the reaction, can adjust their shape according to the adsorption intermediate. In this particular example, the dynamics depend on the size and concentration of the nanoparticles (with a highly complex energy landscape) and also on the temperature of the reaction.

The perspective of dynamic electrocatalysis made us reevaluate the surface curvature effect in a new light of the possibility of geometry adaptive catalysts. An interesting note is that compared to other forms of geometry adaptation, the surface curvature provides a straightforward *linear relation* between geometry and adsorption energy. Thus, it can be considered an ideal model system to explore geometry adaptive catalysis.

6.3.2. Results of geometry adaptive catalysis

Taking previous results from the Sec. 6.2 and augmenting with two new curvatures (4.5 – ideal curvature from fit for $*$OH intermediate, and 21.2 – ideal curvature from fit for $*$O/OH intermediate) provides a dataset to begin the discussion of geometry adaptive catalysts.

First, we can evaluate the fit of the adsorption dependence on curvature, which proved to be rather precise, as indicated by the fact that the newly calculated points almost perfectly correspond to ideal adsorption energies as shown in Fig. 14 (as expected).

Second, we can imagine a catalytic cycle that involves both of these ideal states, illustrated in Fig. 15. This is possible as both of the states have the same *structure*, and the only difference between them is in their *geometry*. In Fig. 16 we consider the FED for the resulting cycle. Notably, the resulting diagram for

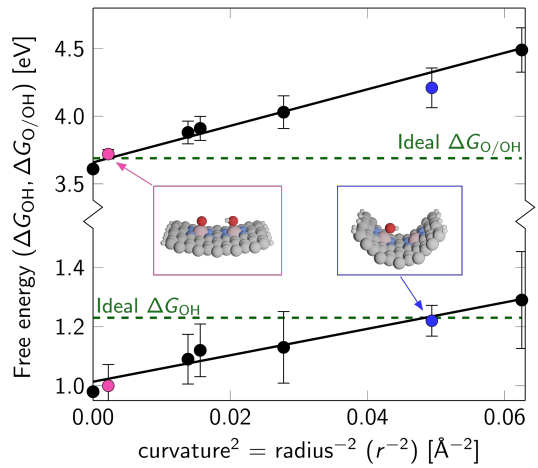

Figure 14. Adsorption energies for 2×CoN_4 model at different curvatures with BEE estimates. The coloured dots indicate the newly calculated points (magenta – curvature radius of 21.2 Å, blue – curvature radius of 4.5 Å).

the adaptive state is almost flat, with some slight deviation from completely flat due to the natural uncertainty in the adsorption energies from the fit. Additionally, we note that the location of blue states, located around 2.6 eV above the magenta states, indicate the energy needed to change between the states.

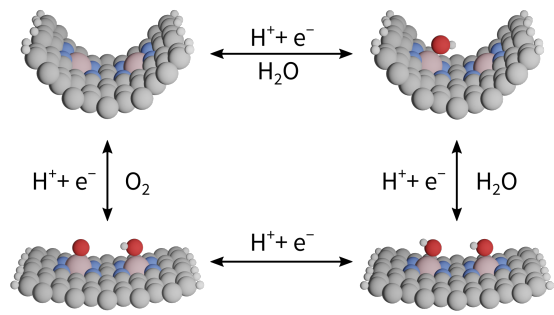

Figure 15. Atomic rendering of geometry adaptive catalysis cycle for oxygen electrocatalysis.

Thus, while it is possible to bypass the scaling relations by having two catalytic states during the reaction. One problem remains – the energy needed to change between the states. Accordingly, in the next section, we explore the effect of the energy needed to change the states to the magnitude of the observed effect in the change of overpotential in more detail.

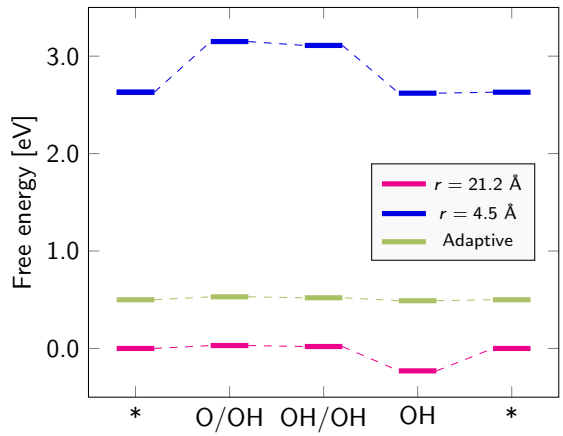

Figure 16. FED at oxygen reduction and evolution equilibrium potential for geometry adaptive catalysis. The energy levels for the adaptive pathway, shown in Fig. 15, are raised in energy by 0.5 eV to distinguish the path graphically.

6.3.3. Pareto analysis

The predicted catalyst, perfectly bypassing scaling relations, requires high curving energy for operation. Herewith, there is an infinite number of switching between other geometric states with a lower curving energy penalty. In Paper III, we considered pairwise combinations of calculated curved states. We showed the overpotential (estimated from scaling relations using fit lines) dependence of curvature energy (energy needed to change between the two states) for a selected range of combinations in Fig. 17. Noticeably, a Pareto front is observed, which describes the trade-off between mechanical (curvature energy) and electrochemical costs (overpotential).

With respect to the Pareto front, one can note two interesting features:

- To reduce the overpotential by around 0.1 V, a significantly less amount of curvature energy of 0.6 eV is necessary. This improvement by 0.1 V is generally comparable to that of other strategies to circumvent scaling relations, and the energy needed is comparable in scale to the relevant energies (e.g. oxygen dissociation energy). Also to note, as previously mentioned, the overpotential estimated from scaling relations is somewhat overestimated when compared to complete FED analysis.
- The slope of the Pareto front has a specific meaning that can be used as a descriptor in geometry adaptive catalysts. In general, the slope corresponds to the "difficulty to change the structure", where catalysts that are easier to geometrically adapt would show steeper slopes. For example, in the ideal case, very little mechanical energy should be needed to achieve zero overpotential.

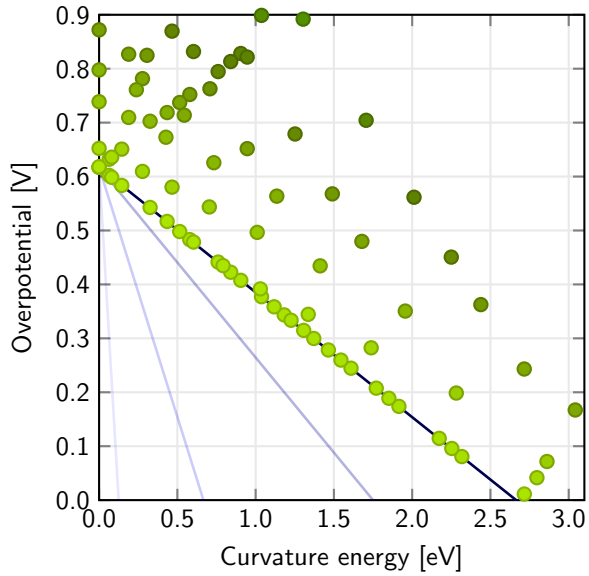

Figure 17. Pareto plot for geometry adaptive catalysts. The markers represent possible combinations of geometric states in the reaction circle, and the colour gradient marks the distance from the Pareto front (marked with a blue line). The transparent blue lines indicate possible improved Pareto fronts for future catalysts.

Even though we exemplify the geometry adaptive catalysis on M–N–C catalysts via surface curvature, other possibilities are imaginable. For example, instead of using the energy of curving (which, unfortunately, is rather high), one can use rotational degrees of freedom of carbon nanotubes or C_{60}, *cis-trans* isomerism from N=N bonds, metal nanocluster rearrangement, and many others [118, 119]. Furthermore, an interesting point to explore in future is whether the curving energy is reversible or irreversible, which likely depends on the catalyst.

6.3.4. Summary and perspectives

We show that geometry adaptive catalysts can potentially bypass the scaling relations and, in theory, reduce the thermodynamic overpotential almost to 0 V. In turn, the limiting factor becomes the energy needed for geometry adaption. Thus, of significant interest is potential research for geometry adaptive catalysts with less energy required to adapt geometry.

7. CONCLUSION

Density functional theory (DFT) calculations have been employed to study the *structural effect* on the CO_2 reduction reaction and the *geometrical effect* on the O_2 reduction reaction. Contrasting these separate studies has revealed a new perspective on discrete and continuous changes in electrocatalysis.

The discrete changes are typical for varying composition and structure, as illustrated by CO_2 reduction to CO and HCOOH at Bi(111) and Bi-N-C surfaces. The modelled *structural effect* clarifies the selectivity observed in bismuth MOF-derived catalysts. Namely, a higher mass content ratio of metal nanoparticles compared to M–N–C species results in higher HCOOH selectivity. From the modelling perspective, this is explained by limiting potentials.

The continuous changes induced by varying geometry (namely curvature) have been predicted for the first time for O_2 reduction at Ni/Co-N-C surfaces with dual-atom sites. This work introduces curvature as a new variable in electrocatalysis. First, the geometrical effect of has been evaluated in the context of strategies to break scaling relations, where it can enable the switching of mechanisms via the *geometrical effect*, resulting in better bifunctional activity and lower overpotentials. Second, based on the revealed linear dependence between curvature and adsorption energy, the principles of geometry adaptive catalysis have been formulated. It is predicted that achieving zero thermodynamic overpotential at the mechanic cost of switching between two geometric states is possible.

A deliberate application of the geometrical effect and experimental realisation of geometry adaptive catalysis can significantly increase the efficiency of crucial reactions: oxygen evolution (in electrolysers and batteries), oxygen reduction (in fuel cells and batteries), carbon dioxide reduction (for power-to-X and carbon neutrality), and nitrogen reduction (for green ammonia production).

BIBLIOGRAPHY

(1) Nørskov, J. K.; Rossmeisl, J.; Logadottir, A.; Lindqvist, L.; Kitchin, J. R.; Bligaard, T.; Jónsson, H. *The Journal of Physical Chemistry B* **2004**, *108*, 17886–17892.

(2) Bligaard, T.; Nørskov, J.; Dahl, S.; Matthiesen, J.; Christensen, C.; Sehested, J. *Journal of Catalysis* **2004**, *224*, 206–217.

(3) Nørskov, J. K.; Bligaard, T.; Logadottir, A.; Kitchin, J. R.; Chen, J. G.; Pandelov, S.; Stimming, U. *Journal of The Electrochemical Society* **2005**, *152*, J23.

(4) Rossmeisl, J.; Logadottir, A.; Nørskov, J. K. *Chemical Physics* **2005**, *319*, 178–184.

(5) Rossmeisl, J.; Skúlason, E.; Björketun, M. E.; Tripković, V.; Nørskov, J. K. *Chemical Physics Letters* **2008**, *466*, 68–71.

(6) Nørskov, J. K.; Bligaard, T.; Rossmeisl, J.; Christensen, C. H. *Nature Chemistry* **2009**, *1*, 37–46.

(7) Rossmeisl, J.; Chan, K.; Ahmed, R.; Tripković, V.; Björketun, M. E. *Physical Chemistry Chemical Physics* **2013**, *15*, 10321.

(8) Rossmeisl, J.; Jensen, K. D.; Petersen, A. S.; Arnarson, L.; Bagger, A.; Escudero-Escribano, M. *The Journal of Physical Chemistry C* **2020**.

(9) Kastlunger, G.; Lindgren, P.; Peterson, A. A. *The Journal of Physical Chemistry C* **2018**, *122*, 12771–12781.

(10) Melander, M. M. *Journal of The Electrochemical Society* **2020**, *167*, 116518.

(11) Kulkarni, A.; Siahrostami, S.; Patel, A.; Nørskov, J. K. *Chemical Reviews* **2018**, *118*, 2302–2312.

(12) Groß, A.; Sakong, S. *Chemical Reviews* **2022**, *122*, 10746–10776.

(13) M, V.; Singh, S.; Bononi, F.; Andreussi, O.; Karmodak, N. *The Journal of Chemical Physics* **2023**, *159*, 111001.

(14) Hofmann, O. T.; Zojer, E.; Hörmann, L.; Jeindl, A.; Maurer, R. J. *Physical Chemistry Chemical Physics* **2021**, *23*, 8132–8180.

(15) Bursch, M.; Mewes, J.-M.; Hansen, A.; Grimme, S. *Angewandte Chemie International Edition* **2022**, *61*, e202205735.

(16) Strmcnik, D.; Uchimura, M.; Wang, C.; Subbaraman, R.; Danilovic, N.; van der Vliet, D.; Paulikas, A. P.; Stamenkovic, V. R.; Markovic, N. M. *Nature Chemistry* **2013**, *5*, 300–306.

(17) Man, I. C.; Su, H.-Y.; Calle-Vallejo, F.; Hansen, H. A.; Martínez, J. I.; Inoglu, N. G.; Kitchin, J.; Jaramillo, T. F.; Nørskov, J. K.; Rossmeisl, J. *ChemCatChem* **2011**, *3*, 1159–1165.

(18) Busch, M.; Halck, N. B.; Kramm, U. I.; Siahrostami, S.; Krtil, P.; Rossmeisl, J. *Nano Energy* **2016**, *29*, 126–135.

(19) Bagger, A.; Christensen, O.; Ivaništšev, V.; Rossmeisl, J. *ACS Catalysis* **2022**, *12*, 2561–2568.

(20) Bratsch, S. G. *Journal of Physical and Chemical Reference Data* **1989**, *18*, 1–21.
(21) Boettcher, S. W.; Oener, S. Z.; Lonergan, M. C.; Surendranath, Y.; Ardo, S.; Brozek, C.; Kempler, P. A. *ACS Energy Letters* **2021**, *6*, 261–266.
(22) Koper, M. T. M. *Chemical Science* **2013**, *4*, 2710–2723.
(23) Göttle, A. J.; Koper, M. T. M. *Chemical Science* **2016**, *8*, 458–465.
(24) Zhang, X.; Li, Y.; Guo, P.; Le, J.-B.; Zhou, Z.-Y.; Cheng, J.; Sun, S.-G. *Journal of Catalysis* **2019**, *376*, 17–24.
(25) Tyburski, R.; Liu, T.; Glover, S. D.; Hammarström, L. *Journal of the American Chemical Society* **2021**, *143*, 560–576.
(26) Schmickler, W. In *Electrochemical Science for a Sustainable Society*, Uosaki, K., Ed., 2017, pp 95–111.
(27) Sakaushi, K.; Kumeda, T.; Hammes-Schiffer, S.; Melander, M. M.; Sugino, O. *Physical Chemistry Chemical Physics* **2020**, *22*, 19401–19442.
(28) Larsen, A. H.; Mortensen, J. J.; Blomqvist, J.; Castelli, I. E.; Christensen, R.; Dulak, M.; Friis, J.; Groves, M. N.; Hammer, B.; Hargus, C.; Hermes, E. D.; Jennings, P. C.; Jensen, P. B.; Kermode, J.; Kitchin, J. R.; Kolsbjerg, E. L.; Kubal, J.; Kaasbjerg, K.; Lysgaard, S.; Maronsson, J. B.; Maxson, T.; Olsen, T.; Pastewka, L.; Peterson, A.; Rostgaard, C.; Schiøtz, J.; Schütt, O.; Strange, M.; Thygesen, K. S.; Vegge, T.; Vilhelmsen, L.; Walter, M.; Zeng, Z.; Jacobsen, K. W. *Journal of Physics: Condensed Matter* **2017**, *29*, 273002.
(29) Head, J. D.; Zerner, M. C. *Chemical Physics Letters* **1985**, *122*, 264–270.
(30) Frederiksen, T.; Paulsson, M.; Brandbyge, M.; Jauho, A.-P. *Physical Review B* **2007**, *75*, 205413.
(31) Mortensen, J. J.; Kaasbjerg, K.; Frederiksen, S. L.; Nørskov, J. K.; Sethna, J. P.; Jacobsen, K. W. *Physical Review Letters* **2005**, *95*, 216401.
(32) Henkelman, G.; Jónsson, H. *The Journal of Chemical Physics* **2000**, *113*, 9978–9985.
(33) Cepitis, R.; Kongi, N.; Grozovski, V.; Ivanistsev, V.; Lust, E. *Catalysts* **2021**, *11*, 1165.
(34) Enkovaara, J.; Rostgaard, C.; Mortensen, J. J.; Chen, J.; Dułak, M.; Ferrighi, L.; Gavnholt, J.; Glinsvad, C.; Haikola, V.; Hansen, H. A.; Kristoffersen, H. H.; Kuisma, M.; Larsen, A. H.; Lehtovaara, L.; Ljungberg, M.; Lopez-Acevedo, O.; Moses, P. G.; Ojanen, J.; Olsen, T.; Petzold, V.; Romero, N. A.; Stausholm-Møller, J.; Strange, M.; Tritsaris, G. A.; Vanin, M.; Walter, M.; Hammer, B.; Häkkinen, H.; Madsen, G. K. H.; Nieminen, R. M.; Nørskov, J. K.; Puska, M.; Rantala, T. T.; Schiøtz, J.; Thygesen, K. S.; Jacobsen, K. W. *Journal of Physics: Condensed Matter* **2010**, *22*, 253202.
(35) Mortensen, J. J.; Larsen, A. H.; Kuisma, M.; Ivanov, A. V.; Taghizadeh, A.; Peterson, A.; Haldar, A.; Dohn, A. O.; Schäfer, C.; Jónsson, E. Ö.;

Hermes, E. D.; Nilsson, F. A.; Kastlunger, G.; Levi, G.; Jónsson, H.; Häkkinen, H.; Fojt, J.; Kangsabanik, J.; Sødequist, J.; Lehtomäki, J.; Heske, J.; Enkovaara, J.; Winther, K. T.; Dulak, M.; Melander, M. M.; Ovesen, M.; Louhivuori, M.; Walter, M.; Gjerding, M.; Lopez-Acevedo, O.; Erhart, P.; Warmbier, R.; Würdemann, R.; Kaappa, S.; Latini, S.; Boland, T. M.; Bligaard, T.; Skovhus, T.; Susi, T.; Maxson, T.; Rossi, T.; Chen, X.; Schmerwitz, Y. L. A.; Schiøtz, J.; Olsen, T.; Jacobsen, K. W.; Thygesen, K. S. *The Journal of Chemical Physics* **2024**, *160*, 092503.

(36) Lejaeghere, K.; Bihlmayer, G.; Björkman, T.; Blaha, P.; Blügel, S.; Blum, V.; Caliste, D.; Castelli, I. E.; Clark, S. J.; Dal Corso, A. *Science* **2016**, *351*, aad3000.

(37) Bosoni, E.; Beal, L.; Bercx, M.; Blaha, P.; Blügel, S.; Bröder, J.; Callsen, M.; Cottenier, S.; Degomme, A.; Dikan, V.; Eimre, K.; Flage-Larsen, E.; Fornari, M.; Garcia, A.; Genovese, L.; Giantomassi, M.; Huber, S. P.; Janssen, H.; Kastlunger, G.; Krack, M.; Kresse, G.; Kühne, T. D.; Lejaeghere, K.; Madsen, G. K. H.; Marsman, M.; Marzari, N.; Michalicek, G.; Mirhosseini, H.; Müller, T. M. A.; Petretto, G.; Pickard, C. J.; Poncé, S.; Rignanese, G.-M.; Rubel, O.; Ruh, T.; Sluydts, M.; Vanpoucke, D. E. P.; Vijay, S.; Wolloch, M.; Wortmann, D.; Yakutovich, A. V.; Yu, J.; Zadoks, A.; Zhu, B.; Pizzi, G. *Nature Reviews Physics* **2024**, *6*, 45–58.

(38) Larsen, A. H.; Kuisma, M.; Löfgren, J.; Pouillon, Y.; Erhart, P.; Hyldgaard, P. *Modelling and Simulation in Materials Science and Engineering* **2017**, *25*, 065004.

(39) Lehtola, S.; Steigemann, C.; Oliveira, M. J. T.; Marques, M. A. L. *SoftwareX* **2018**, *7*, 1–5.

(40) Perdew, J. P.; Burke, K.; Ernzerhof, M. *Physical Review Letters* **1996**, *77*, 3865–3868.

(41) Hammer, B.; Hansen, L. B.; Nørskov, J. K. *Physical Review B* **1999**, *59*, 7413–7421.

(42) Lehtola, S. *The Journal of Chemical Physics* **2023**, *159*.

(43) Wellendorff, J.; Lundgaard, K. T.; Møgelhøj, A.; Petzold, V.; Landis, D. D.; Nørskov, J. K.; Bligaard, T.; Jacobsen, K. W. *Physical Review B* **2012**, *85*, 235149.

(44) Mallikarjun Sharada, S.; Karlsson, R. K. B.; Maimaiti, Y.; Voss, J.; Bligaard, T. *Physical Review B* **2019**, *100*, 035439.

(45) Han, N.; Wang, Y.; Ma, L.; Wen, J.; Li, J.; Zheng, H.; Nie, K.; Wang, X.; Zhao, F.; Li, Y.; Fan, J.; Zhong, J.; Wu, T.; Miller, D. J.; Lu, J.; Lee, S.-T.; Li, Y. *Chem* **2017**, *3*, 652–664.

(46) Granda-Marulanda, L. P.; Rendón-Calle, A.; Builes, S.; Illas, F.; Koper, M. T. M.; Calle-Vallejo, F. *ACS Catalysis* **2020**, *10*, 6900–6907.

(47) Christensen, R.; Bligaard, T.; Jacobsen, K. W. In *Uncertainty Quantification in Multiscale Materials Modeling*, Wang, Y., McDowell, D. L., Eds., 2020, pp 77–91.
(48) Caldeweyher, E.; Mewes, J.-M.; Ehlert, S.; Grimme, S. *Phys. Chem. Chem. Phys.* **2020**, *22*, 8499–8512.
(49) Banisalman, M. J.; Lee, H. W.; Koh, H.; Han, S. S. *ACS Applied Materials & Interfaces* **2021**, *13*, 17577–17585.
(50) Tran, R.; Lan, J.; Shuaibi, M.; Wood, B. M.; Goyal, S.; Das, A.; Heras-Domingo, J.; Kolluru, A.; Rizvi, A.; Shoghi, N.; Sriram, A.; Therrien, F.; Abed, J.; Voznyy, O.; Sargent, E. H.; Ulissi, Z.; Zitnick, C. L. *ACS Catalysis* **2023**, *13*, 3066–3084.
(51) Ringe, S.; Hörmann, N. G.; Oberhofer, H.; Reuter, K. *Chemical Reviews* **2022**, *122*, 10777–10820.
(52) Svane, K. L.; Hansen, H. A.; Vegge, T. *Journal of Catalysis* **2021**, *393*, 230–237.
(53) Calle-Vallejo, F.; Martínez, J. I.; Rossmeisl, J. *Physical Chemistry Chemical Physics* **2011**, *13*, 15639.
(54) Bagger, A.; Castelli, I. E.; Hansen, M. H.; Rossmeisl, J. In *Handbook of Materials Modeling*, Andreoni, W., Yip, S., Eds., 2020, pp 1473–1503.
(55) Sheppard, D.; Terrell, R.; Henkelman, G. *The Journal of Chemical Physics* **2008**, *128*, 134106.
(56) Garrido Torres, J. A.; Jennings, P. C.; Hansen, M. H.; Boes, J. R.; Bligaard, T. *Physical Review Letters* **2019**, *122*, 156001.
(57) Lindgren, P.; Kastlunger, G.; Peterson, A. A. *Journal of Chemical Theory and Computation* **2019**, *15*, 5787–5793.
(58) Wang, X.; Ju, W.; Liang, L.; Riyaz, M.; Bagger, A.; Filippi, M.; Rossmeisl, J.; Strasser, P. *Angewandte Chemie* **2024**, *n/a*, e202401821.
(59) Yang, H.; Wu, Y.; Li, G.; Lin, Q.; Hu, Q.; Zhang, Q.; Liu, J.; He, C. *Journal of the American Chemical Society* **2019**, *141*, 12717–12723.
(60) Zhang, J.; My Pham, T. H.; Gao, Z.; Li, M.; Ko, Y.; Lombardo, L.; Zhao, W.; Luo, W.; Züttel, A. *ACS Catalysis* **2023**, *13*, 9326–9335.
(61) Hepburn, C.; Adlen, E.; Beddington, J.; Carter, E. A.; Fuss, S.; Mac Dowell, N.; Minx, J. C.; Smith, P.; Williams, C. K. *Nature* **2019**, *575*, 87–97.
(62) Cuéllar-Franca, R. M.; Azapagic, A. *Journal of CO2 Utilization* **2015**, *9*, 82–102.
(63) Mac Dowell, N.; Fennell, P. S.; Shah, N.; Maitland, G. C. *Nature Climate Change* **2017**, *7*, 243–249.
(64) Baskaran, D.; Saravanan, P.; Nagarajan, L.; Byun, H.-S. *Chemical Engineering Journal* **2024**, *491*, 151998.
(65) Rajabloo, T.; Valee, J.; Marenne, Y.; Coppens, L.; De Ceuninck, W. *Energy Reports* **2023**, *9*, 111–116.

(66) Sullivan, I.; Goryachev, A.; Digdaya, I. A.; Li, X.; Atwater, H. A.; Vermaas, D. A.; Xiang, C. *Nature Catalysis* **2021**, *4*, 952–958.
(67) Jouny, M.; Luc, W.; Jiao, F. *Nature Catalysis* **2018**, *1*, 748–755.
(68) Machado, A. S. R.; Nunes, A. V. M.; da Ponte, M. N. *The Journal of Supercritical Fluids* **2018**, *134*, 150–156.
(69) Christensen, O.; Bagger, A.; Rossmeisl, J. *ACS Catalysis* **2024**, *14*, 2151–2161.
(70) Valenti, M.; Prasad, N. P.; Kas, R.; Bohra, D.; Ma, M.; Balasubramanian, V.; Chu, L.; Gimenez, S.; Bisquert, J.; Dam, B.; Smith, W. A. *ACS Catalysis* **2019**, *9*, 3527–3536.
(71) Cave, E. R.; Shi, C.; Kuhl, K. P.; Hatsukade, T.; Abram, D. N.; Hahn, C.; Chan, K.; Jaramillo, T. F. *ACS Catalysis* **2018**, *8*, 3035–3040.
(72) Chen, Z.; Zhang, G.; Chen, H.; Prakash, J.; Zheng, Y.; Sun, S. *Renewable and Sustainable Energy Reviews* **2022**, *155*, 111922.
(73) Rendón-Calle, A.; Builes, S.; Calle-Vallejo, F. *Current Opinion in Electrochemistry* **2018**, *9*, 158–165.
(74) Zhu, X.; Li, Y. *WIREs Computational Molecular Science* **2019**, *9*, e1416.
(75) Tang, W.; A. Peterson, A.; Sofia Varela, A.; P. Jovanov, Z.; Bech, L.; J. Durand, W.; Dahl, S.; K. Nørskov, J.; Chorkendorff, I. *Physical Chemistry Chemical Physics* **2012**, *14*, 76–81.
(76) Dinh, C.-T.; Burdyny, T.; Kibria, M. G.; Seifitokaldani, A.; Gabardo, C. M.; García de Arquer, F. P.; Kiani, A.; Edwards, J. P.; De Luna, P.; Bushuyev, O. S.; Zou, C.; Quintero-Bermudez, R.; Pang, Y.; Sinton, D.; Sargent, E. H. *Science* **2018**, *360*, 783–787.
(77) Kwon, Y.; Lum, Y.; Clark, E. L.; Ager, J. W.; Bell, A. T. *ChemElectroChem* **2016**, *3*, 1012–1019.
(78) Abdelkader-Fernández, V. K.; Fernandes, D. M.; Freire, C. *Journal of CO2 Utilization* **2020**, *42*, 101350.
(79) Qiao, J.; Liu, Y.; Hong, F.; Zhang, J. *Chemical Society Reviews* **2014**, *43*, 631.
(80) Oh, W.; Rhee, C. K.; Han, J. W.; Shong, B. *The Journal of Physical Chemistry C* **2018**, *122*, 23084–23090.
(81) Hofmann, Ph. *Progress in Surface Science* **2006**, *81*, 191–245.
(82) Mönig, H.; Sun, J.; Koroteev, Yu. M.; Bihlmayer, G.; Wells, J.; Chulkov, E. V.; Pohl, K.; Hofmann, Ph. *Physical Review B* **2005**, *72*, 085410.
(83) Peterson, A. A.; Abild-Pedersen, F.; Studt, F.; Rossmeisl, J.; K. Nørskov, J. *Energy & Environmental Science* **2010**, *3*, 1311–1315.
(84) Huang, Y.; Zhu, M.; Huang, Y.; Pei, Z.; Li, H.; Wang, Z.; Xue, Q.; Zhi, C. *Advanced Materials* **2016**, *28*, 8344–8364.
(85) Yang, H.; Han, X.; Douka, A. I.; Huang, L.; Gong, L.; Xia, C.; Park, H. S.; Xia, B. Y. *Advanced Functional Materials* **2021**, *31*, 2007602.

(86) Bing, Y.; Liu, H.; Zhang, L.; Ghosh, D.; Zhang, J. *Chemical Society Reviews* **2010**, *39*, 2184–2202.
(87) Geiger, S.; Kasian, O.; Ledendecker, M.; Pizzutilo, E.; Mingers, A. M.; Fu, W. T.; Diaz-Morales, O.; Li, Z.; Oellers, T.; Fruchter, L.; Ludwig, A.; Mayrhofer, K. J. J.; Koper, M. T. M.; Cherevko, S. *Nature Catalysis* **2018**, *1*, 508–515.
(88) Stacy, J.; Regmi, Y. N.; Leonard, B.; Fan, M. *Renewable and Sustainable Energy Reviews* **2017**, *69*, 401–414.
(89) Bhatt, M. D.; Lee, J. Y. *Energy & Fuels* **2020**, *34*, 6634–6695.
(90) Chen, M.-X.; Tong, L.; Liang, H.-W. *Chemistry (Weinheim an Der Bergstrasse, Germany)* **2021**, *27*, 145–157.
(91) Shen, H.; Thomas, T.; Rasaki, S. A.; Saad, A.; Hu, C.; Wang, J.; Yang, M. *Electrochemical Energy Reviews* **2019**, *2*, 252–276.
(92) Kumar, A.; Ibraheem, S.; Anh Nguyen, T.; Gupta, R. K.; Maiyalagan, T.; Yasin, G. *Coordination Chemistry Reviews* **2021**, *446*, 214122.
(93) He, Y.; Liu, S.; Priest, C.; Shi, Q.; Wu, G. *Chemical Society Reviews* **2020**, *49*, 3484–3524.
(94) Shi, Z.; Yang, W.; Gu, Y.; Liao, T.; Sun, Z. *Advanced Science* **2020**, *7*, 2001069.
(95) Wan, H.; Jensen, A. W.; Escudero-Escribano, M.; Rossmeisl, J. *ACS Catalysis* **2020**, *10*, 5979–5989.
(96) Divanis, S.; Kutlusoy, T.; Ingmer Boye, I. M.; Man, I. C.; Rossmeisl, J. *Chemical Science* **2020**, *11*, 2943–2950.
(97) Pérez-Ramírez, J.; López, N. *Nature Catalysis* **2019**, *2*, 971–976.
(98) Huang, Z.-F.; Song, J.; Dou, S.; Li, X.; Wang, J.; Wang, X. *Matter* **2019**, *1*, 1494–1518.
(99) Govindarajan, N.; García-Lastra, J. M.; Meijer, E. J.; Calle-Vallejo, F. *Current Opinion in Electrochemistry* **2018**, *8*, 110–117.
(100) Zhong, L.; Li, S. *ACS Catalysis* **2020**, *10*, 4313–4318.
(101) Exner, K. S. *Materials Horizons* **2023**, *10*, 2086–2095.
(102) Zhao, Y.; Adiyeri Saseendran, D. P.; Huang, C.; Triana, C. A.; Marks, W. R.; Chen, H.; Zhao, H.; Patzke, G. R. *Chemical Reviews* **2023**, *123*, 6257–6358.
(103) Romeo, E.; Illas, F.; Calle-Vallejo, F. *Chemical Science* **2023**, *14*, 3622–3629.
(104) Greeley, J.; Stephens, I. E. L.; Bondarenko, A. S.; Johansson, T. P.; Hansen, H. A.; Jaramillo, T. F.; Rossmeisl, J.; Chorkendorff, I.; Nørskov, J. K. *Nature Chemistry* **2009**, *1*, 552–556.
(105) Peera, S. G.; Liu, C.; Sahu, A. K.; Selvaraj, M.; Rao, M. C.; Lee, T. G.; Koutavarapu, R.; Shim, J.; Singh, L. *Advanced Materials Interfaces* **2021**, *8*, 2100975.

(106) Hong, W. T.; Risch, M.; A. Stoerzinger, K.; Grimaud, A.; Suntivich, J.; Shao-Horn, Y. *Energy & Environmental Science* **2015**, *8*, 1404–1427.
(107) Ibrahim, K. B.; Tsai, M.-C.; Chala, S. A.; Berihun, M. K.; Kahsay, A. W.; Berhe, T. A.; Su, W.-N.; Hwang, B.-J. *Journal of the Chinese Chemical Society* **2019**, *66*, 829–865.
(108) Wang, Y.; Bao, Z.; Shi, M.; Liang, Z.; Cao, R.; Zheng, H. *Chemistry – A European Journal* **2021**, *28*, e202102915.
(109) Li, J.; Xia, W.; Guo, Y.; Qi, R.; Xu, X.; Jiang, D.; Wang, T.; Sugahara, Y.; He, J.; Yamauchi, Y. *Chemical Engineering Journal* **2023**, *477*, 146841.
(110) Su, J.; Musgrave, C. B.; Song, Y.; Huang, L.; Liu, Y.; Li, G.; Xin, Y.; Xiong, P.; Li, M. M.-J.; Wu, H.; Zhu, M.; Chen, H. M.; Zhang, J.; Shen, H.; Tang, B. Z.; Robert, M.; Goddard, W. A.; Ye, R. *Nature Catalysis* **2023**, *6*, 818–828.
(111) Zhu, G.; Li, Y.; Zhu, H.; Su, H.; Chan, S. H.; Sun, Q. *ACS Catalysis* **2016**, *6*, 6294–6301.
(112) Fan, K.; Jia, Y.; Ji, Y.; Kuang, P.; Zhu, B.; Liu, X.; Yu, J. *ACS Catalysis* **2020**, *10*, 358–364.
(113) Wang, Y.; Yang, T.; Fan, X.; Bao, Z.; Tayal, A.; Tan, H.; Shi, M.; Liang, Z.; Zhang, W.; Lin, H.; Cao, R.; Huang, Z.; Zheng, H. *Angewandte Chemie International Edition* **2024**, *63*, e202313034.
(114) Kropp, T.; Mavrikakis, M. *Journal of Catalysis* **2020**, *390*, 67–71.
(115) Feng, Z.; Fang, M.; Li, R.; Ma, B.; Wang, H.; Ding, H.; Su, G.; Tao, K.; Tang, Y.; Dai, X. *International Journal of Hydrogen Energy* **2022**, *47*, 36294–36305.
(116) Ishigami, I.; Sierra, R. G.; Su, Z.; Peck, A.; Wang, C.; Poitevin, F.; Lisova, S.; Hayes, B.; Moss, F. R.; Boutet, S.; Sublett, R. E.; Yoon, C. H.; Yeh, S.-R.; Rousseau, D. L. *Nature Communications* **2023**, *14*, 5752.
(117) Zandkarimi, B.; Alexandrova, A. N. *The Journal of Physical Chemistry Letters* **2019**, *10*, 460–467.
(118) Wang, F.; Xie, L.; Sun, N.; Zhi, T.; Zhang, M.; Liu, Y.; Luo, Z.; Yi, L.; Zhao, Q.; Wang, L. *Nano-Micro Letters* **2023**, *16*, 32.
(119) Jung, S.; Pizzolitto, C.; Biasi, P.; Dauenhauer, P. J.; Birol, T. *Nature Communications* **2023**, *14*, 7795.

ACKNOWLEDGEMENTS

I express great acknowledgement to my supervisors, Assoc. Prof. Nadežda Kongi and Dr. Vladislav Ivaništšev, for the continuous help, always providing learning opportunities and, most importantly, for supporting with the hardest of all – scientific writing.

Also huge thanks to my colleague and friend Akmal Kosimov for many great brainstorming sessions that resulted in surprising research directions and ideas.

I also acknowledge Prof. Jan Rossmeisl for great visiting research opportunities, resulting in refined models and workflows, making the research possible.

I appreciate the computational resources from the University of Tartu HPC Center and the Science HPC Center at the University of Copenhagen that made the research possible. My research work was financially supported by Estonian Research Council (grant PSG250).

SISUKOKKUVÕTE

Struktuuriliste ja geomeetriliste efektide modelleerimine süsinikdioksiidi ja hapniku elektrokatalüüsis

Doktoritöö eesmärk on uurida struktuuriliste ja geomeetriliste muutuste mõju elektrokatalüütilistele reaktsioonidele, kasutades tiheduse funktsionaalse teooria (DFT) arvutusi. Doktoritöö uuringud on keskendunud CO_2 redutseerimisreaktsioonile ja O_2 redutseerimisreaktsioonile, pakkudes uusi perspektiive elektrokatalüüsi diskreetsetele ja pidevatele muutustele.

Diskreetsed muutused on iseloomulikud erineva koostise ja struktuuriga katalüsaatoritele. Näiteks on CO_2 redutseerimist CO-ks ja HCOOH-ks uuritud Bi(111) ja Bi-N-C pindadel. Modelleeritud struktuurilised efektid selgitavad vismuti-põhisest metall orgaanilisest võrestikust saadud katalüsaatorites täheldatud selektiivsust. On leitud, et suurem metalli nanoosakeste massisisaldus võrreldes M-N-C tsentritega toob kaasa kõrgema HCOOH selektiivsuse. Modelleerimise seisukohalt on see seletatav piirpotentsiaali kaudu.

Pidevaid muutusi, mis tulenevad geomeetrilisest erinevusest (eelkõige kõverusest), on ennustatud O_2 redutseerimise reaktsioonil kaheaatomiliste tsentritega Ni/Co-N-C pindadel. Antud doktoritöö tutvustab kõverust kui uut muutujat elektrokatalüüsis. Geomeetrilist efekti hinnatakse skaleerimisseoste katkestamise võime kontekstis, kus see võib võimaldada mehhanismide muutmist geomeetrilise efekti kaudu. Selle tulemusel võib saavutada parema bifunktsionaalse aktiivsuse ja madalama ülepinge.

Lisaks on geomeetrilise kõveruse ja adsorptsioonienergia vahelise lineaarse sõltuvuse põhjal sõnastatud geomeetria kohandamise katalüüsi põhimõtted. Eeldatakse, et termodünaamilise ülepinge nulli saavutamine kahe geomeetrilise oleku vahel vahetamisega on võimalik. Geomeetrilise efekti tahtlik rakendamine ja geomeetria kohandamise katalüüsi eksperimentaalne teostamine võib märkimisväärselt suurendada oluliste reaktsioonide tõhusust, sealhulgas hapniku eraldumine (elektrolüüsiseadmetes ja akudes), hapniku redutseerumine (kütuseelementides ja metal–õhk akudes), süsinikdioksiidi redutseerumine (energiamuundamisseadmed ja süsinikuneutraalsus) ja lämmastiku redutseerumine (rohelise ammoniaagi tootmine). Kokkuvõttes toovad need uuringud esile uued võimalused ja strateegiad elektrokatalüüsi täiustamiseks läbi struktuuriliste ja geomeetriliste muutuste.

PUBLICATIONS

CURRICULUM VITAE

Personal data

Name:	Ritums Cepitis
Born:	14.11.1997
Citizenship:	Latvian
Address:	Ravila 14a, 50411 Tartu, Estonia
E-mail:	ritums.cepitis@ut.ee

Education

2022–...	PhD Student, Institute of Chemistry, University of Tartu, Estonia
2016–2020	University of Cambridge, United Kingdom, M.Sci. & B.A.

Main scientific publications

1. **Cepitis, Ritums**; Ivaništšev, Vladislav; Rossmeisl, Jan; Kongi, Nadezda (2024). Bypassing the scaling relations in oxygen electrocatalysis with geometry-adaptive catalysts. Catalysis Science & Technology, 14, 2105-2113.
   DOI: 10.1039/D4CY00036F
2. **Cepitis, Ritums**; Kongi, Nadezda; Rossmeisl, Jan; Ivaništšev, Vladislav. (2023). Surface Curvature Effect on Dual-Atom Site Oxygen Electrocatalysis. ACS Energy Letters, 8 (3), 1330-1335.
   DOI: 10.1021/acsenergylett.3c00068
3. Kosimov, Akmal; Alimbekova, Amina; Assafrei, Jurgen-Martin; Yusibova, Gulnara; Aruvali, Jaan; Kaarik, Maike; Leis, Jaan; Paiste, Paarn; Ahmadi, Majid; Roohi, Khatereh; Taheri, Peyman; Pinto, Sara M.; **Cepitis, Ritums**; Baptista, Antonio J.; Teppor, Patrick; Lust, Enn; Kongi, Nadezda (2023). Template-Assisted Mechanosynthesis Leading to Benchmark Energy Efficiency and Sustainability in the Production of Bifunctional Fe-N-C Electrocatalysts. ACS Sustainable Chemistry & Engineering, 11 (29), 10825-10834.
   DOI: 10.1021/acssuschemeng.3c02077
4. Ávila-Bolívar, Beatriz; **Cepitis, Ritums**; Alam, Mahboob; Assafrei, Jürgen-Martin; Ping, Kefeng; Aruväli, Jaan; Kikas, Arvo; Kisand, Vambola; Vlassov, Sergei; Käärik, Maike; Leis, Jaan; Ivaništšev, Vladislav; Starkov, Pavel; Montiel, Vicente; Solla-Gullón, José; Kongi, Nadezda (2022). CO2 reduction to formate on an affordable bismuth metal-organic framework based catalyst. Journal of CO2 Utilization, 59, 101937.
   DOI: 10.1016/j.jcou.2022.101937

5. Carrington, Mark E.; Rampal, Nakul; Madden, David G.; O'Nolan, Daniel; Casati, Nicola Pietro Maria; Divitini, Giorgio; Martin-Illan, Jesus A.; Tricarico, Michele; **Cepitis, Ritums**; Camur, Ceren; Curtin, Teresa; Silvestre-Albero, Joaquin; Tan, Jin-Chong; Zamora, Felix; Taraskin, Sergei; Chapman, Karena W.; Fairen-Jimenez, David (2022). Sol-gel processing of a covalent organic framework for the generation of hierarchically porous monolithic adsorbents. Chem, 8 (11), 2961-2977.
DOI: 10.1016/j.chempr.2022.07.013
6. **Cepitis, Ritums**; Kongi, Nadezda; Grozovski, Vitali; Ivanistsev, Vladislav; Lust, Enn (2021). Multifunctional Electrocatalysis on Single-Site Metal Catalysts: A Computational Perspective. Catalysts, 11 (10), 1165.
DOI: 10.3390/catal11101165

ELULOOKIRJELDUS

Isikuandmed

Nimi:	Ritums Cepitis
Sünniaeg:	14.11.1997
Kodakondsus:	Latvian
Aadress:	Ravila 14a, 50411 Tartu, Estonia
E-mail:	ritums.cepitis@ut.ee

Haridus

2022–...	Tartu Ülikool, Loodus- ja täppisteaduste valdkond, Eesti, PhD
2016–2020	Cambridge'i Ülikool, Suurbritannia, MSci & BA

Publikatsioonide loetelu

1. **Cepitis, Ritums**; Ivaništšev, Vladislav; Rossmeisl, Jan; Kongi, Nadezda (2024). Bypassing the scaling relations in oxygen electrocatalysis with geometry-adaptive catalysts. Catalysis Science & Technology, 14, 2105-2113.
   DOI: 10.1039/D4CY00036F
2. **Cepitis, Ritums**; Kongi, Nadezda; Rossmeisl, Jan; Ivaništšev, Vladislav. (2023). Surface Curvature Effect on Dual-Atom Site Oxygen Electrocatalysis. ACS Energy Letters, 8 (3), 1330-1335.
   DOI: 10.1021/acsenergylett.3c00068
3. Kosimov, Akmal; Alimbekova, Amina; Assafrei, Jurgen-Martin; Yusibova, Gulnara; Aruvali, Jaan; Kaarik, Maike; Leis, Jaan; Paiste, Paarn; Ahmadi, Majid; Roohi, Khatereh; Taheri, Peyman; Pinto, Sara M.; **Cepitis, Ritums**; Baptista, Antonio J.; Teppor, Patrick; Lust, Enn; Kongi, Nadezda (2023). Template-Assisted Mechanosynthesis Leading to Benchmark Energy Efficiency and Sustainability in the Production of Bifunctional Fe-N-C Electrocatalysts. ACS Sustainable Chemistry & Engineering, 11 (29), 10825-10834.
   DOI: 10.1021/acssuschemeng.3c02077
4. Ávila-Bolívar, Beatriz; **Cepitis, Ritums**; Alam, Mahboob; Assafrei, Jürgen-Martin; Ping, Kefeng; Aruväli, Jaan; Kikas, Arvo; Kisand, Vambola; Vlassov, Sergei; Käärik, Maike; Leis, Jaan; Ivaništšev, Vladislav; Starkov, Pavel; Montiel, Vicente; Solla-Gullón, José; Kongi, Nadezda (2022). CO2 reduction to formate on an affordable bismuth metal-organic framework based catalyst. Journal of CO2 Utilization, 59, 101937.
   DOI: 10.1016/j.jcou.2022.101937

5. Carrington, Mark E.; Rampal, Nakul; Madden, David G.; O'Nolan, Daniel; Casati, Nicola Pietro Maria; Divitini, Giorgio; Martin-Illan, Jesus A.; Tricarico, Michele; **Cepitis, Ritums**; Camur, Ceren; Curtin, Teresa; Silvestre-Albero, Joaquin; Tan, Jin-Chong; Zamora, Felix; Taraskin, Sergei; Chapman, Karena W.; Fairen-Jimenez, David (2022). Sol-gel processing of a covalent organic framework for the generation of hierarchically porous monolithic adsorbents. Chem, 8 (11), 2961-2977.
DOI: 10.1016/j.chempr.2022.07.013
6. **Cepitis, Ritums**; Kongi, Nadezda; Grozovski, Vitali; Ivanistsev, Vladislav; Lust, Enn (2021). Multifunctional Electrocatalysis on Single-Site Metal Catalysts: A Computational Perspective. Catalysts, 11 (10), 1165.
DOI: 10.3390/catal11101165

DISSERTATIONES CHIMICAE UNIVERSITATIS TARTUENSIS

1. **Toomas Tamm.** Quantum-chemical simulation of solvent effects. Tartu, 1993, 110 p.
2. **Peeter Burk.** Theoretical study of gas-phase acid-base equilibria. Tartu, 1994, 96 p.
3. **Victor Lobanov.** Quantitative structure-property relationships in large descriptor spaces. Tartu, 1995, 135 p.
4. **Vahur Mäemets.** The ^{17}O and ^{1}H nuclear magnetic resonance study of H_2O in individual solvents and its charged clusters in aqueous solutions of electrolytes. Tartu, 1997, 140 p.
5. **Andrus Metsala.** Microcanonical rate constant in nonequilibrium distribution of vibrational energy and in restricted intramolecular vibrational energy redistribution on the basis of slater's theory of unimolecular reactions. Tartu, 1997, 150 p.
6. **Uko Maran.** Quantum-mechanical study of potential energy surfaces in different environments. Tartu, 1997, 137 p.
7. **Alar Jänes.** Adsorption of organic compounds on antimony, bismuth and cadmium electrodes. Tartu, 1998, 219 p.
8. **Kaido Tammeveski.** Oxygen electroreduction on thin platinum films and the electrochemical detection of superoxide anion. Tartu, 1998, 139 p.
9. **Ivo Leito.** Studies of Brønsted acid-base equilibria in water and non-aqueous media. Tartu, 1998, 101 p.
10. **Jaan Leis.** Conformational dynamics and equilibria in amides. Tartu, 1998, 131 p.
11. **Toonika Rinken.** The modelling of amperometric biosensors based on oxidoreductases. Tartu, 2000, 108 p.
12. **Dmitri Panov.** Partially solvated Grignard reagents. Tartu, 2000, 64 p.
13. **Kaja Orupõld.** Treatment and analysis of phenolic wastewater with microorganisms. Tartu, 2000, 123 p.
14. **Jüri Ivask.** Ion Chromatographic determination of major anions and cations in polar ice core. Tartu, 2000, 85 p.
15. **Lauri Vares.** Stereoselective Synthesis of Tetrahydrofuran and Tetrahydropyran Derivatives by Use of Asymmetric Horner-Wadsworth-Emmons and Ring Closure Reactions. Tartu, 2000, 184 p.
16. **Martin Lepiku.** Kinetic aspects of dopamine D_2 receptor interactions with specific ligands. Tartu, 2000, 81 p.
17. **Katrin Sak.** Some aspects of ligand specificity of P2Y receptors. Tartu, 2000, 106 p.
18. **Vello Pällin.** The role of solvation in the formation of iotsitch complexes. Tartu, 2001, 95 p.
19. **Katrin Kollist.** Interactions between polycyclic aromatic compounds and humic substances. Tartu, 2001, 93 p.

20. **Ivar Koppel.** Quantum chemical study of acidity of strong and superstrong Brønsted acids. Tartu, 2001, 104 p.
21. **Viljar Pihl.** The study of the substituent and solvent effects on the acidity of OH and CH acids. Tartu, 2001, 132 p.
22. **Natalia Palm.** Specification of the minimum, sufficient and significant set of descriptors for general description of solvent effects. Tartu, 2001, 134 p.
23. **Sulev Sild.** QSPR/QSAR approaches for complex molecular systems. Tartu, 2001, 134 p.
24. **Ruslan Petrukhin.** Industrial applications of the quantitative structure-property relationships. Tartu, 2001, 162 p.
25. **Boris V. Rogovoy.** Synthesis of (benzotriazolyl)carboximidamides and their application in relations with *N*- and *S*-nucleophyles. Tartu, 2002, 84 p.
26. **Koit Herodes.** Solvent effects on UV-vis absorption spectra of some solvatochromic substances in binary solvent mixtures: the preferential solvation model. Tartu, 2002, 102 p.
27. **Anti Perkson.** Synthesis and characterisation of nanostructured carbon. Tartu, 2002, 152 p.
28. **Ivari Kaljurand.** Self-consistent acidity scales of neutral and cationic Brønsted acids in acetonitrile and tetrahydrofuran. Tartu, 2003, 108 p.
29. **Karmen Lust.** Adsorption of anions on bismuth single crystal electrodes. Tartu, 2003, 128 p.
30. **Mare Piirsalu.** Substituent, temperature and solvent effects on the alkaline hydrolysis of substituted phenyl and alkyl esters of benzoic acid. Tartu, 2003, 156 p.
31. **Meeri Sassian.** Reactions of partially solvated Grignard reagents. Tartu, 2003, 78 p.
32. **Tarmo Tamm.** Quantum chemical modelling of polypyrrole. Tartu, 2003. 100 p.
33. **Erik Teinemaa.** The environmental fate of the particulate matter and organic pollutants from an oil shale power plant. Tartu, 2003. 102 p.
34. **Jaana Tammiku-Taul.** Quantum chemical study of the properties of Grignard reagents. Tartu, 2003. 120 p.
35. **Andre Lomaka.** Biomedical applications of predictive computational chemistry. Tartu, 2003. 132 p.
36. **Kostyantyn Kirichenko.** Benzotriazole – Mediated Carbon–Carbon Bond Formation. Tartu, 2003. 132 p.
37. **Gunnar Nurk.** Adsorption kinetics of some organic compounds on bismuth single crystal electrodes. Tartu, 2003, 170 p.
38. **Mati Arulepp.** Electrochemical characteristics of porous carbon materials and electrical double layer capacitors. Tartu, 2003, 196 p.
39. **Dan Cornel Fara.** QSPR modeling of complexation and distribution of organic compounds. Tartu, 2004, 126 p.
40. **Riina Mahlapuu.** Signalling of galanin and amyloid precursor protein through adenylate cyclase. Tartu, 2004, 124 p.

41. **Mihkel Kerikmäe.** Some luminescent materials for dosimetric applications and physical research. Tartu, 2004, 143 p.
42. **Jaanus Kruusma.** Determination of some important trace metal ions in human blood. Tartu, 2004, 115 p.
43. **Urmas Johanson.** Investigations of the electrochemical properties of polypyrrole modified electrodes. Tartu, 2004, 91 p.
44. **Kaido Sillar.** Computational study of the acid sites in zeolite ZSM-5. Tartu, 2004, 80 p.
45. **Aldo Oras.** Kinetic aspects of dATPαS interaction with $P2Y_1$ receptor. Tartu, 2004, 75 p.
46. **Erik Mölder.** Measurement of the oxygen mass transfer through the air-water interface. Tartu, 2005, 73 p.
47. **Thomas Thomberg.** The kinetics of electroreduction of peroxodisulfate anion on cadmium (0001) single crystal electrode. Tartu, 2005, 95 p.
48. **Olavi Loog.** Aspects of condensations of carbonyl compounds and their imine analogues. Tartu, 2005, 83 p.
49. **Siim Salmar.** Effect of ultrasound on ester hydrolysis in aqueous ethanol. Tartu, 2006, 73 p.
50. **Ain Uustare.** Modulation of signal transduction of heptahelical receptors by other receptors and G proteins. Tartu, 2006, 121 p.
51. **Sergei Yurchenko.** Determination of some carcinogenic contaminants in food. Tartu, 2006, 143 p.
52. **Kaido Tämm.** QSPR modeling of some properties of organic compounds. Tartu, 2006, 67 p.
53. **Olga Tšubrik.** New methods in the synthesis of multisubstituted hydrazines. Tartu. 2006, 183 p.
54. **Lilli Sooväli.** Spectrophotometric measurements and their uncertainty in chemical analysis and dissociation constant measurements. Tartu, 2006, 125 p.
55. **Eve Koort.** Uncertainty estimation of potentiometrically measured ph and pK_a values. Tartu, 2006, 139 p.
56. **Sergei Kopanchuk.** Regulation of ligand binding to melanocortin receptor subtypes. Tartu, 2006, 119 p.
57. **Silvar Kallip.** Surface structure of some bismuth and antimony single crystal electrodes. Tartu, 2006, 107 p.
58. **Kristjan Saal.** Surface silanization and its application in biomolecule coupling. Tartu, 2006, 77 p.
59. **Tanel Tätte.** High viscosity $Sn(OBu)_4$ oligomeric concentrates and their applications in technology. Tartu, 2006, 91 p.
60. **Dimitar Atanasov Dobchev**. Robust QSAR methods for the prediction of properties from molecular structure. Tartu, 2006, 118 p.
61. **Hannes Hagu**. Impact of ultrasound on hydrophobic interactions in solutions. Tartu, 2007, 81 p.
62. **Rutha Jäger.** Electroreduction of peroxodisulfate anion on bismuth electrodes. Tartu, 2007, 142 p.

63. **Kaido Viht.** Immobilizable bisubstrate-analogue inhibitors of basophilic protein kinases: development and application in biosensors. Tartu, 2007, 88 p.
64. **Eva-Ingrid Rõõm.** Acid-base equilibria in nonpolar media. Tartu, 2007, 156 p.
65. **Sven Tamp.** DFT study of the cesium cation containing complexes relevant to the cesium cation binding by the humic acids. Tartu, 2007, 102 p.
66. **Jaak Nerut.** Electroreduction of hexacyanoferrate(III) anion on Cadmium (0001) single crystal electrode. Tartu, 2007, 180 p.
67. **Lauri Jalukse.** Measurement uncertainty estimation in amperometric dissolved oxygen concentration measurement. Tartu, 2007, 112 p.
68. **Aime Lust.** Charge state of dopants and ordered clusters formation in CaF_2:Mn and CaF_2:Eu luminophors. Tartu, 2007, 100 p.
69. **Iiris Kahn**. Quantitative Structure-Activity Relationships of environmentally relevant properties. Tartu, 2007, 98 p.
70. **Mari Reinik.** Nitrates, nitrites, N-nitrosamines and polycyclic aromatic hydrocarbons in food: analytical methods, occurrence and dietary intake. Tartu, 2007, 172 p.
71. **Heili Kasuk.** Thermodynamic parameters and adsorption kinetics of organic compounds forming the compact adsorption layer at Bi single crystal electrodes. Tartu, 2007, 212 p.
72. **Erki Enkvist.** Synthesis of adenosine-peptide conjugates for biological applications. Tartu, 2007, 114 p.
73. **Svetoslav Hristov Slavov**. Biomedical applications of the QSAR approach. Tartu, 2007, 146 p.
74. **Eneli Härk.** Electroreduction of complex cations on electrochemically polished Bi(*hkl*) single crystal electrodes. Tartu, 2008, 158 p.
75. **Priit Möller.** Electrochemical characteristics of some cathodes for medium temperature solid oxide fuel cells, synthesized by solid state reaction technique. Tartu, 2008, 90 p.
76. **Signe Viggor.** Impact of biochemical parameters of genetically different pseudomonads at the degradation of phenolic compounds. Tartu, 2008, 122 p.
77. **Ave Sarapuu.** Electrochemical reduction of oxygen on quinone-modified carbon electrodes and on thin films of platinum and gold. Tartu, 2008, 134 p.
78. **Agnes Kütt.** Studies of acid-base equilibria in non-aqueous media. Tartu, 2008, 198 p.
79. **Rouvim Kadis.** Evaluation of measurement uncertainty in analytical chemistry: related concepts and some points of misinterpretation. Tartu, 2008, 118 p.
80. **Valter Reedo.** Elaboration of IVB group metal oxide structures and their possible applications. Tartu, 2008, 98 p.
81. **Aleksei Kuznetsov.** Allosteric effects in reactions catalyzed by the cAMP-dependent protein kinase catalytic subunit. Tartu, 2009, 133 p.

82. **Aleksei Bredihhin.** Use of mono- and polyanions in the synthesis of multisubstituted hydrazine derivatives. Tartu, 2009, 105 p.
83. **Anu Ploom.** Quantitative structure-reactivity analysis in organosilicon chemistry. Tartu, 2009, 99 p.
84. **Argo Vonk.** Determination of adenosine A_{2A}- and dopamine D_1 receptor-specific modulation of adenylate cyclase activity in rat striatum. Tartu, 2009, 129 p.
85. **Indrek Kivi.** Synthesis and electrochemical characterization of porous cathode materials for intermediate temperature solid oxide fuel cells. Tartu, 2009, 177 p.
86. **Jaanus Eskusson.** Synthesis and characterisation of diamond-like carbon thin films prepared by pulsed laser deposition method. Tartu, 2009, 117 p.
87. **Marko Lätt.** Carbide derived microporous carbon and electrical double layer capacitors. Tartu, 2009, 107 p.
88. **Vladimir Stepanov.** Slow conformational changes in dopamine transporter interaction with its ligands. Tartu, 2009, 103 p.
89. **Aleksander Trummal.** Computational Study of Structural and Solvent Effects on Acidities of Some Brønsted Acids. Tartu, 2009, 103 p.
90. **Eerold Vellemäe.** Applications of mischmetal in organic synthesis. Tartu, 2009, 93 p.
91. **Sven Parkel.** Ligand binding to 5-HT_{1A} receptors and its regulation by Mg^{2+} and Mn^{2+}. Tartu, 2010, 99 p.
92. **Signe Vahur.** Expanding the possibilities of ATR-FT-IR spectroscopy in determination of inorganic pigments. Tartu, 2010, 184 p.
93. **Tavo Romann**. Preparation and surface modification of bismuth thin film, porous, and microelectrodes. Tartu, 2010, 155 p.
94. **Nadežda Aleksejeva.** Electrocatalytic reduction of oxygen on carbon nanotube-based nanocomposite materials. Tartu, 2010, 147 p.
95. **Marko Kullapere.** Electrochemical properties of glassy carbon, nickel and gold electrodes modified with aryl groups. Tartu, 2010, 233 p.
96. **Liis Siinor.** Adsorption kinetics of ions at Bi single crystal planes from aqueous electrolyte solutions and room-temperature ionic liquids. Tartu, 2010, 101 p.
97. **Angela Vaasa.** Development of fluorescence-based kinetic and binding assays for characterization of protein kinases and their inhibitors. Tartu 2010, 101 p.
98. **Indrek Tulp.** Multivariate analysis of chemical and biological properties. Tartu 2010, 105 p.
99. **Aare Selberg.** Evaluation of environmental quality in Northern Estonia by the analysis of leachate. Tartu 2010, 117 p.
100. **Darja Lavõgina.** Development of protein kinase inhibitors based on adenosine analogue-oligoarginine conjugates. Tartu 2010, 248 p.
101. **Laura Herm.** Biochemistry of dopamine D_2 receptors and its association with motivated behaviour. Tartu 2010, 156 p.

102. **Terje Raudsepp.** Influence of dopant anions on the electrochemical properties of polypyrrole films. Tartu 2010, 112 p.
103. **Margus Marandi.** Electroformation of Polypyrrole Films: *In-situ* AFM and STM Study. Tartu 2011, 116 p.
104. **Kairi Kivirand.** Diamine oxidase-based biosensors: construction and working principles. Tartu, 2011, 140 p.
105. **Anneli Kruve.** Matrix effects in liquid-chromatography electrospray mass-spectrometry. Tartu, 2011, 156 p.
106. **Gary Urb.** Assessment of environmental impact of oil shale fly ash from PF and CFB combustion. Tartu, 2011, 108 p.
107. **Nikita Oskolkov.** A novel strategy for peptide-mediated cellular delivery and induction of endosomal escape. Tartu, 2011, 106 p.
108. **Dana Martin.** The QSPR/QSAR approach for the prediction of properties of fullerene derivatives. Tartu, 2011, 98 p.
109. **Säde Viirlaid.** Novel glutathione analogues and their antioxidant activity. Tartu, 2011, 106 p.
110. **Ülis Sõukand.** Simultaneous adsorption of Cd^{2+}, Ni^{2+}, and Pb^{2+} on peat. Tartu, 2011, 124 p.
111. **Lauri Lipping.** The acidity of strong and superstrong Brønsted acids, an outreach for the "limits of growth": a quantum chemical study. Tartu, 2011, 124 p.
112. **Heisi Kurig.** Electrical double-layer capacitors based on ionic liquids as electrolytes. Tartu, 2011, 146 p.
113. **Marje Kasari.** Bisubstrate luminescent probes, optical sensors and affinity adsorbents for measurement of active protein kinases in biological samples. Tartu, 2012, 126 p.
114. **Kalev Takkis.** Virtual screening of chemical databases for bioactive molecules. Tartu, 2012, 122 p.
115. **Ksenija Kisseljova**. Synthesis of aza-β^3-amino acid containing peptides and kinetic study of their phosphorylation by protein kinase A. Tartu, 2012, 104 p.
116. **Riin Rebane.** Advanced method development strategy for derivatization LC/ESI/MS. Tartu, 2012, 184 p.
117. **Vladislav Ivaništšev.** Double layer structure and adsorption kinetics of ions at metal electrodes in room temperature ionic liquids. Tartu, 2012, 128 p.
118. **Irja Helm.** High accuracy gravimetric Winkler method for determination of dissolved oxygen. Tartu, 2012, 139 p.
119. **Karin Kipper.** Fluoroalcohols as Components of LC-ESI-MS Eluents: Usage and Applications. Tartu, 2012, 164 p.
120. **Arno Ratas.** Energy storage and transfer in dosimetric luminescent materials. Tartu, 2012, 163 p.
121. **Reet Reinart-Okugbeni**. Assay systems for characterisation of subtype-selective binding and functional activity of ligands on dopamine receptors. Tartu, 2012, 159 p.

122. **Lauri Sikk.** Computational study of the Sonogashira cross-coupling reaction. Tartu, 2012, 81 p.
123. **Karita Raudkivi.** Neurochemical studies on inter-individual differences in affect-related behaviour of the laboratory rat. Tartu, 2012, 161 p.
124. **Indrek Saar.** Design of GalR2 subtype specific ligands: their role in depression-like behavior and feeding regulation. Tartu, 2013, 126 p.
125. **Ann Laheäär.** Electrochemical characterization of alkali metal salt based non-aqueous electrolytes for supercapacitors. Tartu, 2013, 127 p.
126. **Kerli Tõnurist.** Influence of electrospun separator materials properties on electrochemical performance of electrical double-layer capacitors. Tartu, 2013, 147 p.
127. **Kaija Põhako-Esko.** Novel organic and inorganic ionogels: preparation and characterization. Tartu, 2013, 124 p.
128. **Ivar Kruusenberg.** Electroreduction of oxygen on carbon nanomaterial-based catalysts. Tartu, 2013, 191 p.
129. **Sander Piiskop.** Kinetic effects of ultrasound in aqueous acetonitrile solutions. Tartu, 2013, 95 p.
130. **Ilona Faustova**. Regulatory role of L-type pyruvate kinase N-terminal domain. Tartu, 2013, 109 p.
131. **Kadi Tamm.** Synthesis and characterization of the micro-mesoporous anode materials and testing of the medium temperature solid oxide fuel cell single cells. Tartu, 2013, 138 p.
132. **Iva Bozhidarova Stoyanova-Slavova.** Validation of QSAR/QSPR for regulatory purposes. Tartu, 2013, 109 p.
133. **Vitali Grozovski**. Adsorption of organic molecules at single crystal electrodes studied by *in situ* STM method. Tartu, 2014, 146 p.
134. **Santa Veikšina**. Development of assay systems for characterisation of ligand binding properties to melanocortin 4 receptors. Tartu, 2014, 151 p.
135. **Jüri Liiv.** PVDF (polyvinylidene difluoride) as material for active element of twisting-ball displays. Tartu, 2014, 111 p.
136. **Kersti Vaarmets.** Electrochemical and physical characterization of pristine and activated molybdenum carbide-derived carbon electrodes for the oxygen electroreduction reaction. Tartu, 2014, 131 p.
137. **Lauri Tõntson**. Regulation of G-protein subtypes by receptors, guanine nucleotides and Mn^{2+}. Tartu, 2014, 105 p.
138. **Aiko Adamson.** Properties of amine-boranes and phosphorus analogues in the gas phase. Tartu, 2014, 78 p.
139. **Elo Kibena**. Electrochemical grafting of glassy carbon, gold, highly oriented pyrolytic graphite and chemical vapour deposition-grown graphene electrodes by diazonium reduction method. Tartu, 2014, 184 p.
140. **Teemu Näykki.** Novel Tools for Water Quality Monitoring – From Field to Laboratory. Tartu, 2014, 202 p.
141. **Karl Kaupmees.** Acidity and basicity in non-aqueous media: importance of solvent properties and purity. Tartu, 2014, 128 p.

142. **Oleg Lebedev**. Hydrazine polyanions: different strategies in the synthesis of heterocycles. Tartu, 2015, 118 p.
143. **Geven Piir.** Environmental risk assessment of chemicals using QSAR methods. Tartu, 2015, 123 p.
144. **Olga Mazina.** Development and application of the biosensor assay for measurements of cyclic adenosine monophosphate in studies of G protein-coupled receptor signalinga. Tartu, 2015, 116 p.
145. **Sandip Ashokrao Kadam.** Anion receptors: synthesis and accurate binding measurements. Tartu, 2015, 116 p.
146. **Indrek Tallo.** Synthesis and characterization of new micro-mesoporous carbide derived carbon materials for high energy and power density electrical double layer capacitors. Tartu, 2015, 148 p.
147. **Heiki Erikson.** Electrochemical reduction of oxygen on nanostructured palladium and gold catalysts. Tartu, 2015, 204 p.
148. **Erik Anderson.** *In situ* Scanning Tunnelling Microscopy studies of the interfacial structure between Bi(111) electrode and a room temperature ionic liquid. Tartu, 2015, 118 p.
149. **Girinath G. Pillai.** Computational Modelling of Diverse Chemical, Biochemical and Biomedical Properties. Tartu, 2015, 140 p.
150. **Piret Pikma.** Interfacial structure and adsorption of organic compounds at Cd(0001) and Sb(111) electrodes from ionic liquid and aqueous electrolytes: an *in situ* STM study. Tartu, 2015, 126 p.
151. **Ganesh babu Manoharan.** Combining chemical and genetic approaches for photoluminescence assays of protein kinases. Tartu, 2016, 126 p.
152. **Carolin Siimenson**. Electrochemical characterization of halide ion adsorption from liquid mixtures at Bi(111) and pyrolytic graphite electrode surface. Tartu, 2016, 110 p.
153. **Asko Laaniste.** Comparison and optimisation of novel mass spectrometry ionisation sources. Tartu, 2016, 156 p.
154. **Hanno Evard.** Estimating limit of detection for mass spectrometric analysis methods. Tartu, 2016, 224 p.
155. **Kadri Ligi.** Characterization and application of protein kinase-responsive organic probes with triplet-singlet energy transfer. Tartu, 2016, 122 p.
156. **Margarita Kagan.** Biosensing penicillins' residues in milk flows. Tartu, 2016, 130 p.
157. **Marie Kriisa.** Development of protein kinase-responsive photoluminescent probes and cellular regulators of protein phosphorylation. Tartu, 2016, 106 p.
158. **Mihkel Vestli.** Ultrasonic spray pyrolysis deposited electrolyte layers for intermediate temperature solid oxide fuel cells. Tartu, 2016, 156 p.
159. **Silver Sepp**. Influence of porosity of the carbide-derived carbon on the properties of the composite electrocatalysts and characteristics of polymer electrolyte fuel cells. Tartu, 2016, 137 p.
160. **Kristjan Haav**. Quantitative relative equilibrium constant measurements in supramolecular chemistry. Tartu, 2017, 158 p.

161. **Anu Teearu**. Development of MALDI-FT-ICR-MS methodology for the analysis of resinous materials. Tartu, 2017, 205 p.
162. **Taavi Ivan**. Bifunctional inhibitors and photoluminescent probes for studies on protein complexes. Tartu, 2017, 140 p.
163. **Maarja-Liisa Oldekop**. Characterization of amino acid derivatization reagents for LC-MS analysis. Tartu, 2017, 147 p.
164. **Kristel Jukk**. Electrochemical reduction of oxygen on platinum- and palladium-based nanocatalysts. Tartu, 2017, 250 p.
165. **Siim Kukk**. Kinetic aspects of interaction between dopamine transporter and *N*-substituted nortropane derivatives. Tartu, 2017, 107 p.
166. **Birgit Viira**. Design and modelling in early drug development in targeting HIV-1 reverse transcriptase and Malaria. Tartu, 2017, 172 p.
167. **Rait Kivi**. Allostery in cAMP dependent protein kinase catalytic subunit. Tartu, 2017, 115 p.
168. **Agnes Heering**. Experimental realization and applications of the unified acidity scale. Tartu, 2017, 123 p.
169. **Delia Juronen**. Biosensing system for the rapid multiplex detection of mastitis-causing pathogens in milk. Tartu, 2018, 85 p.
170. **Hedi Rahnel.** ARC-inhibitors: from reliable biochemical assays to regulators of physiology of cells. Tartu, 2018, 176 p.
171. **Anton Ruzanov.** Computational investigation of the electrical double layer at metal–aqueous solution and metal–ionic liquid interfaces. Tartu, 2018, 129 p.
172. **Katrin Kestav.** Crystal Structure-Guided Development of Bisubstrate-Analogue Inhibitors of Mitotic Protein Kinase Haspin. Tartu, 2018, 166 p.
173. **Mihkel Ilisson.** Synthesis of novel heterocyclic hydrazine derivatives and their conjugates. Tartu, 2018, 101 p.
174. **Anni Allikalt.** Development of assay systems for studying ligand binding to dopamine receptors. Tartu, 2018, 160 p.
175. **Ove Oll.** Electrical double layer structure and energy storage characteristics of ionic liquid based capacitors. Tartu, 2018, 187 p.
176. **Rasmus Palm.** Carbon materials for energy storage applications. Tartu, 2018, 114 p.
177. **Jörgen Metsik.** Preparation and stability of poly(3,4-ethylenedioxythiophene) thin films for transparent electrode applications. Tartu, 2018, 111 p.
178. **Sofja Tšepelevitš.** Experimental studies and modeling of solute-solvent interactions. Tartu, 2018, 109 p.
179. **Märt Lõkov.** Basicity of some nitrogen, phosphorus and carbon bases in acetonitrile. Tartu, 2018, 104 p.
180. **Anton Mastitski**. Preparation of α-aza-amino acid precursors and related compounds by novel methods of reductive one-pot alkylation and direct alkylation. Tartu, 2018, 155 p.
181. **Jürgen Vahter**. Development of bisubstrate inhibitors for protein kinase CK2. Tartu, 2019, 186 p.

182. **Piia Liigand.** Expanding and improving methodology and applications of ionization efficiency measurements. Tartu, 2019, 189 p.
183. **Sigrid Selberg.** Synthesis and properties of lipophilic phosphazene-based indicator molecules. Tartu, 2019, 74 p.
184. **Jaanus Liigand.** Standard substance free quantification for LC/ESI/MS analysis based on the predicted ionization efficiencies. Tartu, 2019, 254 p.
185. **Marek Mooste.** Surface and electrochemical characterisation of aryl film and nanocomposite material modified carbon and metal-based electrodes. Tartu, 2019, 304 p.
186. **Mare Oja.** Experimental investigation and modelling of pH profiles for effective membrane permeability of drug substances. Tartu, 2019, 306 p.
187. **Sajid Hussain.** Electrochemical reduction of oxygen on supported Pt catalysts. Tartu, 2019, 220 p.
188. **Ronald Väli.** Glucose-derived hard carbon electrode materials for sodium-ion batteries. Tartu, 2019, 180 p.
189. **Ester Tee.** Analysis and development of selective synthesis methods of hierarchical micro- and mesoporous carbons. Tartu, 2019, 210 p.
190. **Martin Maide.** Influence of the microstructure and chemical composition of the fuel electrode on the electrochemical performance of reversible solid oxide fuel cell. Tartu, 2020, 144 p.
191. **Edith Viirlaid.** Biosensing Pesticides in Water Samples. Tartu, 2020, 102 p.
192. **Maike Käärik.** Nanoporous carbon: the controlled nanostructure, and structure-property relationships. Tartu, 2020, 162 p.
193. **Artur Gornischeff.** Study of ionization efficiencies for derivatized compounds in LC/ESI/MS and their application for targeted analysis. Tartu, 2020, 124 p.
194. **Reet Link.** Ligand binding, allosteric modulation and constitutive activity of melanocortin-4 receptors. Tartu, 2020, 108 p.
195. **Pilleriin Peets.** Development of instrumental methods for the analysis of textile fibres and dyes. Tartu, 2020, 150 p.
196. **Larisa Ivanova.** Design of active compounds against neurodegenerative diseases. Tartu, 2020, 152 p.
197. **Meelis Härmas.** Impact of activated carbon microstructure and porosity on electrochemical performance of electrical double-layer capacitors. Tartu, 2020, 122 p.
198. **Ruta Hecht.** Novel Eluent Additives for LC-MS Based Bioanalytical Methods. Tartu, 2020, 202 p.
199. **Max Hecht.** Advances in the Development of a Point-of-Care Mass Spectrometer Test. Tartu, 2020, 168 p.
200. **Ida Rahu.** Bromine formation in inorganic bromide/nitrate mixtures and its application for oxidative aromatic bromination. Tartu, 2020, 116 p.
201. **Sander Ratso**. Electrocatalysis of oxygen reduction on non-precious metal catalysts. Tartu, 2020, 371 p.
202. **Astrid Darnell.** Computational design of anion receptors and evaluation of host-guest binding. Tartu, 2021, 150 p.

203. **Ove Korjus.** The development of ceramic fuel electrode for solid oxide cells. Tartu, 2021, 150 p.
204. **Merit Oss.** Ionization efficiency in electrospray ionization source and its relations to compounds' physico-chemical properties. Tartu, 2021, 124 p.
205. **Madis Lüsi**. Electroreduction of oxygen on nanostructured palladium catalysts. Tartu, 2021, 180 p.
206. **Eliise Tammekivi.** Derivatization and quantitative gas-chromatographic analysis of oils. Tartu, 2021, 122 p.
207. **Simona Selberg.** Development of Small-Molecule Regulators of Epi-transcriptomic Processes. Tartu, 2021, 122 p.
208. **Olivier Etebe Nonga.** Inhibitors and photoluminescent probes for in vitro studies on protein kinases PKA and PIM. Tartu, 2021, 189 p.
209. **Riinu Härmas.** The structure and H2 diffusion in porous carbide-derived carbon particles. Tartu, 2022, 123 p.
210. **Maarja Paalo.** Synthesis and characterization of novel carbon electrodes for high power density electrochemical capacitors. Tartu, 2022, 144 p.
211. **Jinfeng Zhao.** Electrochemical characteristics of Bi(hkl) and micro-meso-porous carbon electrodes in ionic liquid based electrolytes. Tartu, 2022, 134 p.
212. **Alar Heinsaar.** Investigation of oxygen electrode materials for high-temperature solid oxide cells in natural conditions. Tartu, 2022, 120 p.
213. **Jaana Lilloja.** Transition metal and nitrogen doped nanocarbon cathode catalysts for anion exchange membrane fuel cells. Tartu, 2022, 202 p.
214. **Maris-Johanna Tahk.** Novel fluorescence-based methods for illuminating transmembrane signal transduction by G-protein coupled receptors. Tartu, 2022, 200 p.
215. **Eerik Jõgi.** Development and Applications of E. coli Immunosensor. Tartu, 2022, 103 p.
216. **Alo Rüütel.** Design principles of synthetic molecular receptors for anion-selective electrodes. Tartu, 2022, 109 p.
217. **Tanel Sõrmus.** Development of stimuli-responsive and covalent bisubstrate inhibitors of protein kinases. Tartu, 2022, 148 p.
218. **Oleg Artemchuk.** Autotrophic nitrogen removal processes for nutrient removal from sidestream and mainstream wastewater. Tartu, 2022, 115 p.
219. **Andre Leesment.** Quantitative studies of Brønsted acidity in biphasic systems and gas-phase. Tartu, 2023, 83 p.
220. **Meeli Arujõe-Sado.** Structural effects in aza-peptide bond formation reaction. Tartu, 2023, 83 p.
221. **Jonas Mart Linge.** Electrochemical reduction of oxygen on silver-based catalysts. Tartu, 2023, 269 p.
222. **Tõnis Laasfeld.** Integrating Image Analysis and Quantitative Modeling for a Holistic View of GPCR Ligand Binding Dynamics. Tartu, 2023, 226 p.
223. **Ernesto de Jesus Zapata Flores.** Derivatization Reagents used in negative mode electrospray LC-MS. Tartu, 2023, 107 p.

224. **Patrick Teppor.** Obtaining platinum-free oxygen reduction catalysts through biomass valorization: a case study of peat. Tartu, 2023, 161 p.
225. **Peeter Valk.** Methanol Oxidation on Platinum-Rare-Earth Metal Oxide Activated Catalysts. Tartu, 2023, 162 p.
226. **Shidong Chen.** Unravelling prehistoric plant exploitation in eastern Baltic: organic residue analysis of plant-based materials by multi-method approach. Tartu, 2023, 245 p.
227. **Yogesh Kumar.** M-N_4 macrocycle-based catalysts for electrocatalysis of oxygen reduction and oxygen evolution. Tartu, 2023, 224 p.
228. **Kerli Martin.** Recognition of carboxylates by synthetic receptors – from structure-affinity studies to solid-contact anion-selective electrode prototyping. Tartu, 2023, 130 p.
229. **Huy Quí Vinh Nguyen.** Development of Carbon Supported Pt–CeO_2 Catalysts for Proton Exchange Membrane Fuel Cells. Tartu, 2023, 198 p.
230. **Heigo Ers**. Adsorption and Structuring Processes at Single Crystal Electrode – Ionic Liquid Interface – Insights from Simulations and *in situ* Studies. Tartu, 2024, 137 p.